COMPARATIVE IN SILICO ANALYSIS OF THE ANTIVIRAL POTENTIAL OF ISOLATED COMPOUNDS AND GC-MS EXTRACTS OF ARTEMISIA ANNUA AGAINST 5RMM PROTEIN OF SARS-CoV-2

BY

KPANDO SUSAN

PHA1908535

SUPERVISED BY

DR. VINCENT O. IMIEJE

DEPARTMENT OF PHARMACEUTICAL CHEMISTRY

FACULTY OF PHARMACY

UNIVERSITY OF BENIN

BENIN CITY

NOVEMBER, 2025.

COMPARATIVE IN SILICO ANALYSIS OF THE ANTIVIRAL POTENTIAL OF ISOLATED COMPOUNDS AND GC-MS EXTRACTS OF ARTEMISIA ANNUA AGAINST 5RMM PROTEIN OF SARS-CoV-2

BY

KPANDO SUSAN IJEOMA

PHA1908535

A DISSERTATION SUBMITTED TO THE DEPARTMENT OF PHARMACEUTICAL CHEMISTRY, FACULTY OF PHARMACY, UNIVERSITY OF BENIN, BENIN CITY, IN PARTIAL FULFILMENT OF THE REQUIREMENT FOR THE AWARD OF DOCTOR OF PHARMACY (PHARM.D) DEGREE HONOURS OF THE UNIVERSITY OF BENIN, BENIN CITY, EDO STATE, NIGERIA.

NOVEMBER, 2025.

CERTIFICATION

This is to certify that this work was done by Kpando Susan Ijeoma in the Department of Pharmaceutical Chemistry, Faculty of Pharmacy, University of Benin, Benin City, Nigeria, in partial fulfillment of the requirements of the award of the Doctor of Pharmacy Degree

(Pharm. D).

_____ _____

Dr. Vincent O. Imieje Date

(Project Supervisor)

_____ _____

Dr. Vincent O. Imieje Date

(Head of Department)

_____ _____

Kpando Susan Ijeoma Date

(Student)

DEDICATION

This work is dedicated to God Almighty and my Family. Thank you for everything.

ACKNOWLEDGEMENTS

Firstly, my utmost thanks and gratitude go to God Almighty, El Hayyay, my Father and my Friend, without whom none of this would have even started or been completed. For being my Strength in my times of weakness, I'm so grateful, Lord. Thank you.

Special thanks to my Project Supervisor, Dr. Vincent O. Imieje. It's because you believed in me, listened to and answered all my questions, provided all the support I needed, and consistently pushed me to be and do better that I have this work to present. Thank you also to all my teammates for this project, Edesiri, Ayomide, Nelson, and Bamidele. Thank you for answering my numerous questions and providing consistent support

I'm also grateful to my family. Thank you, Mum and Dad, for all your support, spiritual, financial, emotional, and otherwise. I could never have gotten this far if I didn't always believe that you had my back. Thank you, Chukwudumebi and Divine, for advising me every two weeks that I should stop being a crybaby and finish what I started. Thank you, Olisaemeka. God bless you all abundantly.

Special thanks to Dr. Uyi Ogbeide Dr. Isioma Ogbeide, and to EL-TETMAC Pharmacy, for being a haven where I could rest all my worries, both academic and otherwise, and all my fears, and for being a turning point in my life. I'm forever grateful for everything; words can't even begin to explain.

Lastly, thank you to all my friends, Setale, Stephanie, Didi, Regina, Vanessa, Elaine, Habby, and Jeymar. Thank you for being my safe space and holding me up in times I couldn't support myself. This journey was a lot easier because I had you all. Thank you, Ebuka for all the songs and memories. Thank you, Joshua, for doing even more than I expected every single time. You're a star. I'm very grateful.

TABLE OF CONTENTS

LIST OF TABLES

TABLE OF FIGURES

LIST OF ABBREVIATIONS

ACE2: Angiotensin-Converting Enzyme 2

ADMET: Absorption, Distribution, Metabolism, Excretion, and Toxicity

CADD: Computer-Aided Drug Design

CID: Compound ID (used in PubChem to identify chemical substances)

COVID-19: Coronavirus Disease 2019

CT: Computed Tomography

FDA: Food and Drug Administration

GC-MS: Gas Chromatography–Mass Spectrometry

hACE2: Human Angiotensin-Converting Enzyme 2

HIV: Human Immunodeficiency Virus

LBDD: Ligand-Based Drug Design

LBVS: Ligand-Based Virtual Screening

LD50: Lethal Dose 50%

MERS-CoV: Middle East Respiratory Syndrome Coronavirus

MLOGP: Octanol-Water Partition Coefficient (SwissADME model)

NSP: Non-Structural Protein

ORF: Open Reading Frame

PDB: Protein Data Bank

PLIP: Protein–Ligand Interaction Profiler

ROS: Reactive Oxygen Species

RTC: Replication and Transcription Complex

S: Spike Protein

SARS-CoV-2: Severe Acute Respiratory Syndrome Coronavirus 2

SBDD: Structure-Based Drug Design

SBVS: Structure-Based Virtual Screening

VS: Virtual Screening

ABSTRACT

SARS-CoV-2, an RNA virus from the Coronaviridae family, remains a global threat due to its rapid variant evolution and immune evasion. *Artemisia annua* is used traditionally to treat malaria and has documented antiviral activity. This study assesses the inhibitory potential of *A. annua* extracts against the SARS-CoV-2 helicase 5RMM responsible for viral replication using computational and biochemical methods. Phytoconstituents present in this plant were obtained from literature sources as well as GC-MS analysis. Their 3D structures were obtained from PubChem; the protein helicase (5RMM) was retrieved from the Protein Data Bank (PDB) and processed using Biovia Discovery Studio 2025. Molecular docking was performed using PyRx. Post-docking analysis was done using Biovia Discovery Studio 2025, and ADMET profiling was conducted using the Swiss ADME web server and Pro-Tox 3.0 virtual lab.

Eighteen (18) phytoconstituents from the isolated compounds showed low ΔG energy <-7 kcal/mol. Others have ΔG energy <-6.5 kcal/mol. Post-docking analysis and ADMET profiling of the ligands showed that Quercimeritrin and Rhamnetin were identified as putative drug molecules based on their high binding affinity and hydrogen-bond interactions with the target protein's active-site amino acid residues. Deoxyartemisinin from the n-Hexane extract and 3H-Cyclodeca[b]furan-2-one,4,9-dihydroxy-6-methyl-3,10-dimethylene-3a,4,7,8,9,10,11,11a-octahydro- from the dichloromethane extract were also highlighted for their high binding affinity scores. Isolated compounds, especially flavonols from *Artemisia annua,* demonstrate notable *in-silico* antiviral activity against SARS-CoV-2. Findings suggest the therapeutic potential of these compounds. Further investigation is required to confirm the compounds' efficacy, elucidate their molecular mechanisms of action, and assess their safety across diverse biological systems.

CHAPTER ONE

1.1 INTRODUCTION

1.1.1 OVERVIEW OF THE VIRAL DISEASE COVID-19 AND THE CAUSATIVE VIRUS SARS-CoV-2

The virus known as severe acute respiratory syndrome coronavirus 2 (SARS-CoV-2), commonly referred to as "the novel coronavirus" because of its genetic differences from earlier identified coronaviruses, is a positive-sense RNA virus responsible for COVID-19. SARS-CoV-2 is classified within the Coronaviridae family and the Coronavirinae subfamily, comprising large, single-stranded RNA viruses that have an envelope and range in size from 65 to 125 nm in diameter. When observed under electron microscopy, the virions appear approximately spherical and have protruding structures (glycoproteins) on their surface, which are typically called spikes. These spikes resemble a crown (or “corona” in Latin), which is the origin of the name for this group of viruses. So far, only seven coronaviruses are known to infect humans. Four of them (comprising two α-CoVs and two β-CoVs) result in mild, cold-like symptoms, whereas three, including severe acute respiratory syndrome coronavirus (SARS-CoV), Middle East respiratory syndrome coronavirus (MERS-CoV), and the recently identified SARS-CoV-2, can cause severe or deadly illness. (Emrani, J., *et al*. 2021). SARS-CoV-2 shares an 80% phylogenetic similarity with severe acute respiratory syndrome coronavirus (SARS-CoV) and has a 50% resemblance to Middle East respiratory syndrome coronavirus (MERS-CoV), both of which triggered worldwide outbreaks in 2002–2003 and 2011, respectively (Muralidar, S., *et al*, 2020). SARS-CoV-2 appeared in 2019, resulting in the ongoing global pandemic.

1.1.2 PATHOGENESIS AND TRANSMISSION

The primary mechanism for the transmission of SARS-CoV-2 involves infected respiratory droplets, necessitating direct, indirect, or close contact with individuals who are infected (Muralidar, S., *et al*., 2020). At a molecular level, the virus employs the angiotensin-converting enzyme 2 (ACE2) for cellular entry, mirroring the receptor usage of SARS-CoV (Turner, A. J., 2015). This receptor, identified as a zinc metalloenzyme and ectoenzyme on endothelial surfaces

such as in the lungs, is targeted by the viral spike (S) protein (Khailany, R. A., *et al*., 2020). This transmembrane protein is composed of two subunits: the S1 subunit, responsible for receptor binding, and the S2 subunit, which facilitates fusion with the host cell membrane. A significant factor in the virus's potential for cross-species transmission is its ability to recognize ACE2 receptors not only in humans (hACE2) but also in a diverse range of animals, including pigs, ferrets, cats, and pangolins. This broad receptor specificity suggests a wide host range for SARS-CoV-2, with the varying efficiency of ACE2 usage across different species likely influencing their relative susceptibility to infection.

The clinical presentation of SARS-CoV-2 infection ranges widely, from mild, nonspecific symptoms to life-threatening respiratory failure. The disease process initiates when the virus binds to respiratory tract epithelial cells, commencing replication and subsequently progressing downward through the airways to infiltrate alveolar epithelial cells in the lungs. This robust viral replication within lung tissue can provoke an exaggerated immune reaction. In severe cases, this dysregulated response escalates into a cytokine storm syndrome, which can precipitate acute respiratory distress syndrome (ARDS). Ultimately, this cascade of events leading to respiratory failure is identified as the principal cause of mortality in COVID-19 patients. (Hu *et al.,* 2021)

Following an incubation period of approximately five days, infected hosts become contagious and can readily transmit the virus to others via respiratory exhalation. The symptomatic presentation of COVID-19 arises from transient damage inflicted upon susceptible host cells. This cellular injury can occur across multiple organ systems, notably impacting the lungs, intestines, kidneys, and blood vessels.(Gu and Korteweg *et al,* 2007)

1.1.3 DIAGNOSIS

The molecular identification of SARS-CoV-2 nucleic acid remains the diagnostic benchmark. Commercially available kits commonly target genomic regions such as the ORF1b (which includes the RdRp gene), N, E, or S genes, with detection times varying from minutes to several hours based on the specific technological platform (Hu *et al*., 2021). A wide range of sample types can yield a positive identification, including tracheal aspirates, bronchoalveolar lavage, pleural fluids, urine, blood, and faeces. Notably, viral RNA can persist in anal and faecal swabs for weeks after respiratory samples return a negative result. Saliva is also emerging as a viable

diagnostic medium for detecting both the virus and virus-specific antibodies, potentially serving as a practical standard for screening in high-throughput scenarios like air or sea travel. A positive salivary antigen test indicates active infection (El-Daly, 2024). However, the potential for false negatives—particularly with oral swabs—necessitates a multi-faceted diagnostic approach. Consequently, for patients with a high clinical suspicion of COVID-19 but an initial negative nucleic acid test, it is recommended to employ chest CT scanning in conjunction with repeated swab testing (Xie *et al*., 2020).

1.1.4 GLOBAL IMPACT OF COVID-19

Global surveillance data from the World Health Organization, current as of August 9, 2025, has documented over 760 million confirmed cases and 6.9 million fatalities attributable to COVID-19 since its emergence in December 2019, though these figures are widely considered an undercount (WHO, 2025). The heightened transmissibility of SARS-CoV-2 relative to prior coronaviruses like SARS-CoV (2002) and MERS-CoV (2012) stems from key virological and epidemiological factors. A critical aspect is the potential for re-infection, which is facilitated by the virus's sophisticated mechanisms for evading host immune responses. This adaptive capacity is evidenced by the continual emergence of new variants. Notable examples, such as the Alpha (B.1.1.7), Beta (B.1.351), Delta (B.1.617.2), and Gamma (P.1) lineages, demonstrated increased contagiousness and virulence. While many of these earlier variants have since been de-escalated in monitoring systems like the EU's as of June 27, 2025, the persistent circulation of variants of interest, such as Omicron (BA.2.86), underscores the virus's rapid evolution to enhance its infectiousness and circumvent established immunity (ECDC, 2025).

1.1.5 THERAPEUTICS OF COVID-19

Potentially controversial medications that block the entry of SARS-CoV-2 include the antimalarial medication chloroquine and its derivative hydroxychloroquine. These drugs are used for both the prevention and treatment of malaria and autoimmune disorders, such as systemic lupus erythematosus and rheumatoid arthritis. They function by inhibiting the glycosylation of cell receptors and the binding between the virus and host receptors, increasing the endosomal pH, and hindering membrane fusion. Currently, their effectiveness in treating COVID-19 continues to

be a topic of debate. In vitro studies have shown that they can prevent SARS-CoV-2 infection (Wang *et al*., 2020), although clinical findings are not definitive. Despite this discovery, these medications

should be used with caution because they are known to cause a variety of adverse reactions and drug-drug interactions that could negatively impact disease progression. In cases of overdose, chloroquine and hydroxychloroquine can also be extremely toxic (Juurlink, 2020). On June 15, 2020, the US Food and Drug Administration (FDA) revoked the emergency use authorization for chloroquine and hydroxychloroquine in the treatment of COVID-19 due to their side effects.

An alternative treatment approach could involve inhibiting the viral replication of SARS-CoV-2. One of the repurposed medications currently utilized for COVID-19 is the combination of Lopinavir and Ritonavir. These drugs are protease inhibitors that are used in the management of HIV infections. They are suggested to inhibit the SARS-CoV 3C-like protease enzyme, which is considered crucial for processing coronavirus polyproteins. Their use is primarily based on previous experiences with Lopinavir and Ritonavir during SARS and MERS outbreaks. A systematic review assessing the outcomes of Lopinavir-Ritonavir treatment in SARS and MERS patients indicated better clinical results and a reduced risk of ARDS or mortality. However, this evidence largely derives from case reports and retrospective studies (Patel *et al*., 2021). Remdesivir is a broad-spectrum antiviral that has shown efficacy against multiple viruses, including filoviruses (such as Ebola and Marburg), coronaviruses (like SARS-CoV, MERS-CoV, and SARS-CoV-2), paramyxoviruses (such as parainfluenza type III, Nipah, Hendra, measles, and mumps), and Pneumoviridae (like respiratory syncytial virus). Laboratory studies have indicated that it possesses antiviral properties against SARS-CoV-2, which led to its investigation as a potential treatment at the beginning of the pandemic. Nonetheless, it has not demonstrated effectiveness in randomized clinical trials, and its efficacy either on its own or in combination with other drugs has not been examined against the variants of SARS-CoV-2, as there is always a concern about resistance development with antiviral medications faced with mutant viruses (Aleem and Kothadia, 2022). This underscores the need for further comprehensive research into the potential for novel therapies to work concurrently to manage the virus effectively.

1.1.6 THE VIRAL PROTEIN 5RMM

The SARS-CoV-2 virion contains a single-stranded RNA genome of 29,811 nucleotides, which provides the blueprint for 29 distinct viral proteins. This genetic scale is minuscule compared to the human genome, which comprises approximately 3.2 billion nucleotides and codes for an estimated 20,000 proteins. Phylogenetically classified as a novel betacoronavirus, SARS-CoV-2 demonstrates a 79% genetic sequence identity with SARS-CoV and 50% with MERS-CoV. Its genomic organization follows the characteristic betacoronavirus pattern: the 5' to 3' arrangement of open reading frames (ORFs) includes the large replicase polyprotein (ORF1a/ORF1b) followed by the genes for the four primary structural proteins—spike (S), envelope (E), membrane (M), and nucleocapsid (N). Interspersed among these are seven hypothetical ORFs that encode accessory proteins. While the lengths of most SARS-CoV-2 proteins are comparable to their SARS-CoV counterparts, the structural genes show particularly high conservation, sharing over 90% amino acid identity. The key exception is the spike (S) protein, which is the most divergent. At 1,273 amino acids, the SARS-CoV-2 S protein is longer than both the SARS-CoV S protein (1,255 aa) and those found in bat SARS-related coronaviruses (1,245–1,269 aa), a feature that may contribute to its distinct functional properties (Hu *et al*., 2021).

All viral proteins associated with SARS-CoV-2 can be classified into three groups: 1) structural proteins, 2) non-structural proteins, or 3) accessory proteins (Emrani *et al*, 2021). SARS-CoV-2 possesses 16 non-structural proteins (Nsps), along with polyproteins, nucleoproteins, and membrane proteins, each fulfilling distinct roles. Most of these non-structural proteins of SARS-CoV-2 exhibit more than 85 percent similarity in amino acid sequence with those of SARS-CoV (Hu *et al*, 2021).

The protein being discussed here is the 5RMM or Nsp13 protein, a 67 kDa non-structural protein classified within the helicase superfamily 1B. It utilizes the energy derived from nucleotide triphosphate hydrolysis to facilitate the unwinding of double-stranded DNA or RNA in a 5' to 3' manner. NSP13 comprises five domains: a N-terminal domain, a Zinc-binding domain (ZBD) that houses three structural zinc ions, a helical stalk domain, a beta-barrel 1B domain, and two 'RecA-like' helicase subdomains, namely 1A and 2A, which contain the residues necessary for nucleotide binding and cleavage into smaller components (Newman *et al*., 2021). Given the contrasting polarity of helicase translocation moving 5′ to 3′ in comparison to polymerase,

NSP13 is thought to be involved in processes such as backtracking, template switching, or the disruption of secondary structures downstream (Chen *et al*., 2020). The SARS-CoV-2 virus possesses two mini versions of its replication and transcription complex (RTC), each featuring different conformations of NSP13 (NSP13-1 and NSP13-2). In both RTC copies, NSP13-1 contributes to stabilizing the overall structure of the mini RTC by interacting with NSP13-2, which serves to anchor the 5′-extension of the RNA template, as well as forming connections with the NSP7-NSP8-NSP12-RNA complex (Yan *et al*., 2020).

Although the precise function of NSP13 in the viral life cycle remains largely unknown, it has been identified as a crucial element in viral replication for SARS-CoV and other more distantly related viral families. The most conserved non-structural protein within the SARS-CoV-2 genome is NSP13, which differs from SARS-CoV by only a single amino acid substitution (V570I). This high level of conservation suggests that SARS-CoV, along with potentially other future coronaviruses, may respond similarly to treatments targeting NSP13 (Newman *et al*., 2021). Ideally, a therapeutically active treatment for COVID-19 would also be effective against previous and yet-to-emerge coronaviruses. For a pharmacological agent to effectively inhibit NSP13, it would need to target a highly conserved binding site shared across all coronaviruses, thereby serving as a broad-spectrum inhibitor. Examination of the druggability and significance of its binding pockets has shown that the binding pocket occupied by the 5′-end of the RNA substrate is both druggable and significantly conserved. Consequently, it represents a promising candidate for developing broad-spectrum inhibitors against future coronaviruses.

1.1.7 NATURAL PRODUCT-BASED DRUG DISCOVERY: AN OVERVIEW

The rational investigation of plant-derived drugs, while building upon a rich historical foundation, commenced in earnest during the early 19th century. This pivotal shift was triggered by Friedrich Sertürner, a German apothecary assistant, who successfully isolated the potent analgesic and soporific component of opium. He named the compound "morphium" (morphine) after Morpheus, the Greek god of dreams. Sertürner's seminal paper detailed its isolation, crystallization, structural characteristics, and pharmacological effects, which he had preliminarily investigated in stray dogs before progressing to self-experimentation. This breakthrough served

as a catalyst, spurring the systematic study of other medicinal herbs. Throughout the subsequent decades, a wave of bioactive natural products—predominantly alkaloids such as quinine, caffeine, nicotine, and cocaine—were isolated and could be produced in substantial quantities. This new ability gave rise to the modern pharmaceutical industry, which originated in apothecaries specializing in purifying these compounds. The first of these was H.E. Merck in Darmstadt, Germany, which initiated the commercial extraction of morphine and other alkaloids in 1826. The next logical advancement was the pursuit of chemical synthesis to produce these compounds with higher quality and at a lower cost, a milestone first achieved with the synthesis of salicylic acid in 1853 (Atanasov *et al*., 2015). According to two review studies, among the 1073 new chemical entities approved from 1981 to 2010 within the category of small molecules, just 36 percent were completely synthetic, while the remainder were either discovered or motivated by natural sources, with many originating from higher plants. (Newman *et al*.,2012; Kinghorn *et al*., 2011).

Modern pharmacotherapy continues to rely heavily on plant-derived compounds, a dependence starkly illustrated by several cornerstone treatments. In oncology, for instance, agents like vincristine and vinblastine from the Madagascar periwinkle (Catharanthus roseus (L.) G. Don), paclitaxel from yew (Taxus) species, and camptothecin from Camptotheca acuminata Decne. form the backbone of many chemotherapeutic protocols. The influence extends to other therapeutic areas, exemplified by galanthamine, a cholinesterase inhibitor for Alzheimer's disease sourced from the snowdrop (Galanthus nivalis L.) (Lim et al., 2024), and artemisinin, a potent antimalarial from Artemisia annua L. that also shows promise as an anti-cancer agent (Atanasov *et al*., 2015)

The pharmaceutical industry has always been drawn to natural products, and the consideration of plant-derived drugs and other alternative treatments is driven by numerous reasons. Synthetic medicines are quick-fixing but there are a lot of negative effects that come along with them. Synthetic medicine is an expensive product because it is produced in a complex process and could be out of reach for the great majority of the global population. Conversely, the traditional medicines are generally safe, more effective with few side effects, and are readily metabolised and absorbed by the body. They are highly acceptable, cheap, and readily available to the people because of their cultural and social beliefs. Scientific research and clinical trials have offered

evidence-based medicines, developed by scientists and pharmaceutical companies. In addition, purification and standardization of a single compound are more convenient and thus easily allow its applications in the modern drug delivery system. (Nasim *et al*., 2022)

1.1.8 ARTEMISIA ANNUA AND SARS-CoV-2

Also known as sweet wormwood, sweet annie, sweet sagewort, annual mugwort, or annual wormwood (Wikipedia, 2025). Artemisia annua is an annual herb plant, thus the name "*annua"*.It belongs to the family of Asteraceae. In Asia, Central and Eastern Europe, the temperate parts of America, Africa, and Australia, and the tropical areas, the plant is cultivated. It is consumed as a food spice, as herbal tea, and as a medicinal plant in the Asian mild climates, like in China and Korea. (Septembre-Malaterre *et al*., 2020). Annua is a shrub that is large with a single stem having alternating branches, which sometimes extends up to 2.0 m in height. It lacks a woody stem. The shrub fragrantly divides its 2.5-5 cm long aromatic leaves. The leaves and the flowers have biseriate trichomes, ten-celled and filamentous trichomes, which are five-celled. Macroscopically, the plant, *A. annua,* is fragrant and has deeply grooved branches. As a rule, there is a variation in the leaf and aerial parts. The margins of the leaves are not ideal, and yet the base is asymmetrical. The leaf changes its color from light to dark green and has a pinnate arrangement. The external as well as the internal areas are globes. The surfaces contain both lobular and nonglandular trichomes. The spongy parenchyma is composed of four to six layers of freely packed cells. Its physicochemical analysis, however, reveals that it has 9.2 w/w moisture, 8.3 w/w total ash, 0.91 percent acid-insoluble ash, 6.2 w/w alcohol, and 3.8 v/w water. The leaves and inflorescence of the plant contain a high percentage of protein, crude fat, and digestible fractions. Plant tissue contains manganese and copper in abundance. Moreover, this herb is of high nutritional value due to its rich amino acid and vitamin composition (Swamikannu *et al*., 2024). For many years, traditional medicine in Asia and Africa has utilized it to treat malaria and fever. The infusion of the dried herb is recognized as a remedy for fever and malaria in the current pharmacopoeia of the People's Republic of China, with recommended doses ranging from 4.5 to 9 grams per day. This herbal formulation is primarily employed in clinical trials for research purposes. Since its discovery, extensive research has been conducted on the chemical composition of Artemisia annua. Over 600 secondary metabolites have been identified within the plant, including numerous sesquiterpenoids, triterpenoids, monoterpenoids,

steroids, flavonoids, coumarins, alkaloids, and benzenoids. The chemical makeup and biological properties of the aqueous or alcoholic extracts of Artemisia annua can differ significantly based on factors such as geographical origin, the type of plant material used, and the treatment method applied, unlike its essential oil, which shows only minor variations. (Septembre-Malaterre *et al*., 2020)

Figure 1.1 The plant of interest, Artemisia annua

Artemisia annua, due to its vast phytochemical library, also has a variety of pharmacological uses; studies have shown its antipyretic, antiseptic, antispasmodic, carminative, anti-inflammatory, antidiabetic, hypolipidemic, anti-helminthic, antioxidant, antimicrobial, and anti-cancerous activity. The most notable one, though, would be its antimalarial activity, which is carried out by the sesquiterpene lactone, Artemisinin, which targets *Plasmodium falciparum*, the causative organism of malaria. Artemisinin and its derivatives have also been shown to have antiviral activity against human cytomegalovirus, Epstein-Barr virus, herpes simplex virus 1, and human herpes virus 6A, hepatitis B and C virus, and HIV-1 virus. (Verma *et al*., 2020). Moreover, the potential of artemisinin against SARS-CoV-2 was also confirmed by a study (Cao *et al*., 2020) that evaluated the activities of nine artemisinin-related compounds for their anti-SARS-CoV-2 activity in vitro, establishing a pharmacokinetic model that can predict the therapeutic potential of selected compounds against SARS-CoV-2. These studies have laid the foundation for further research into the activity of Artemisia annua against SARS-CoV-2, suggesting that other secondary compounds in this plant have the ability to exhibit anti-SARS-CoV-2 activity. Besides

antiviral compound-potential compounds, the *A. annua* secondary metabolites profiles also indicated an appropriate amount of antioxidant molecules in the leaves. Such results are suitable because the main complications that plague individuals during and after the COVID-19 pandemic are explained by the presence of oxidative stress, which appears as a result of the imbalance between the generation and elimination of free radicals during the SARS-CoV-2 infection. Infectious diseases and viral replication are caused by damage through excessive generation of reactive oxygen species (ROS), like an insufficient response of antioxidants and excessive lipid peroxidation. In this case, antiviral action and antioxidant effects of *A. annua* can contribute to the effect and neutralize the inflammatory reaction in COVID-19. (Baggieri *et al*., 2023). A detailed review study (Fuzimoto, 2021) has shown the strong inhibitory effect of different compounds of *Artemisia annua* on several essential viral proteins of SARS-CoV-2. Four out of the total number of studies reviewed were in vitro, fourteen were *in silico*, and one article was a controlled clinical trial. However, the critical analysis of the literature it encompasses reveals that this study predominantly focused on a limited set of viral targets and mechanisms. Crucially, the potential of *A. annua*-derived compounds, whether well-characterized isolates or constituents within complex extracts, to inhibit the essential SARS-CoV-2 non-structural protein 13 (NSP13) helicase remained virtually unexplored. Recent work by Corona *et al*. (2022) addressed the inhibitory potential of natural compounds against SARS-CoV-2 NSP13 helicase, identifying several flavonoids with promising activity. However, their study focused on a limited compound set and did not explore the broader phytochemical diversity of *Artemisia annua*. Considering that it has already been established prior in this paper that NSP13 (5RMM) is a highly conserved and indispensable motor protein for viral replication and is recognized as a premium target for broad-spectrum anti-coronaviral therapy, the absence of dedicated research to this specific protein indicates a critical missing link in fully elucidating the complete activity of *Artemisia annua* against SARS-CoV-2.

To further expand our understanding of the possible antiviral properties of Artemisia annua, this research intends to assess and compare the antiviral effectiveness of both well-known isolated compounds of Artemisia annua and the various phytochemical components found in two sets of its GC-MS extracts against the SARS-CoV-2 helicase protein NSP13 (5RMM), utilizing a thorough comparative in-silico method. In light of the increasing evidence supporting the

inhibitory effects of flavonoids on NSP13, this investigation particularly emphasizes flavonoid-rich components, along with coumarins and phenolic acids, with the goal of identifying potential, effective lead targets for further experimental exploration for pharmacotherapeutic applications. The choice to concentrate on flavonoids in this analysis is additionally backed by recent structural findings from Kloskowski *et al*. (2025), who elucidated the crystal structure of the SARS-CoV-2 NSP13 in association with the natural flavonoid myricetin. Their research uncovered a conserved allosteric binding site on NSP13 that fits myricetin, showing that this interaction hinders the helicase's RNA-unwinding function. These findings not only confirm NSP13 as a viable target for drug development but also highlight the mechanistic significance of flavonoids as potential inhibitors. Building upon this information, our research broadens its scope by examining a wider array of flavonoids and phytochemicals derived from Artemisia annua, with the aim of discovering new NSP13 inhibitors that possess greater pharmacotherapeutic potential.

1.1.9 COMPUTER-AIDED DRUG DESIGN

Recognizing and creating a new therapeutic agent can be a labor-intensive and costly process in the broad field of drug discovery, and as a result, this journey mainly depended on chance findings or conventional trial-and-error approaches, frequently taking decades and considerable resources without a certain result. The introduction of Computer-Aided Drug Design (CADD), which combines the detailed complexities of biological systems with the forecasting capabilities of computational algorithms, along with the creation of databases curated with chemical and biological data, represented a significant advancement in the 20th century in terms of drug discovery. The fundamental concept behind CADD involves applying computer algorithms to chemical and biological data to model and anticipate the interactions between a drug molecule and its target, typically a protein or DNA sequence within a biological context. This can vary from analyzing the molecular structure of the drug or its target and estimating how the drug will attach to the target, and also predicting its pharmacological effects and any possible side effects.

1.1.9.1 BENEFITS OF CADD

Computer-Aided Drug Design is a methodology that fosters the use of computational tools and techniques for the creation and identification of new viable therapeutic agents, while ensuring the efficient use of resources allocated to computational research. In recent years, it has progressed significantly, enhancing our comprehension of intricate biological mechanisms and allowing for the faster development of new therapeutically active compounds. Additionally, the implementation of *in-silico* filters, like the Lipinski rule, helps assess drug-likeness and pharmacokinetic properties, filtering out molecules that do not possess characteristics consistent with an ideal, druggable pharmacotherapeutic agent, thereby streamlining the drug discovery process. It also offers detailed insights into the interactions between drugs/ligands and receptors. (Purohit *et al*, 2022)

1.1.9.2 CATEGORIES OF CADD

Computer-Aided Drug Design (CADD) is fundamentally categorized into structure-based (SBDD) and ligand-based (LBDD) approaches (Niazi and Mariam, 2023). The prerequisite for SBDD is a three-dimensional structure of the biological target, typically elucidated through techniques like X-ray crystallography, nuclear magnetic resonance (NMR) spectroscopy, or single-particle cryo-electron microscopy (cryo-EM). With a known structure as a foundation, in silico studies can be employed to pinpoint potential ligands that possess the desired therapeutic characteristics. Following these computational simulations, the most promising candidates are synthesized. Their biological properties, including affinity, potency, and efficacy, are then rigorously evaluated through a variety of experimental assays. (Ferreira *et al*.,2015).

Following the identification of active compounds, the three-dimensional structure of the resulting ligand-receptor complex can be determined. In contrast to Structure-Based Drug Design (SBDD), the Ligand-Based Drug Design (LBDD) approach functions without prior knowledge of the therapeutic target's structure, relying instead on structural and bioactivity data from known small molecules. The foundational premise of LBDD is that structural similarity among compounds often predicts similar biological properties. Consequently, a central component of its methodology involves curating libraries of small molecules and identifying a lead compound from within them (Sharma *et al*., 2021). SBDD is now indispensable for the efficient creation of

new therapeutics and for elucidating metabolic pathways. Its methodology, which is grounded in the use of a target's three-dimensional structure, has proven more effective than conventional high-throughput screening. Utilizing computational tools and 3D protein data, SBDD allows researchers to investigate critical molecular interactions governing ligand binding, thereby enabling the interpretation of experimental results with molecular precision. Advanced SBDD techniques, such as virtual screening (VS) and *de novo* drug design, offer a more targeted and efficient paradigm than traditional high-throughput screening (Lionta *et al*., 2014).

1.1.9.3 VIRTUAL SCREENING

Virtual screening is a cornerstone technique in medicinal chemistry for the discovery of lead compounds. This process computationally evaluates vast libraries of drug-like molecules against a biological target with a known three-dimensional structure. The core of this screening is molecular docking, which ranks ligands according to their predicted binding affinity. The most promising candidates identified in silico are then prioritized for in vitro testing to confirm their biological activity. There are two principal categories of virtual screening: ligand-based (LBVS) and structure-based (SBVS). LBVS leverages known biological data to distinguish active from inactive molecules, applying tools such as consensus pharmacophores, similarity searches, and molecular descriptors to pinpoint highly active chemical scaffolds. Conversely, SBVS requires a priori knowledge of the target protein's 3D structure. This approach computationally analyzes the target against extensive compound libraries, using scoring functions to estimate the binding energy of docked complexes—predictions that are subsequently validated through experimental assays. This scoring of ligands is a fundamental component of SBVS, a key distinction being that, unlike LBVS, structure-based methods do not depend on pre-existing experimental data for similar compounds (Batool *et al*., 2019).

1.1.9.4 MOLECULAR DOCKING

At its core, molecular docking computationally simulates atomic-level interactions between a protein and a small molecule ligand. The primary objective of this technique is twofold: first, to determine the ligand's preferred binding mode (its pose), including its conformation, location, and orientation within the protein's active site; and second, to quantitatively score the stability of that pose through an estimated binding affinity (Meng *et al*., 2011). To achieve this, docking programs rely on conformational search algorithms that explore possible ligand poses. These algorithms generally operate on either systematic or stochastic principles and form the computational engine of various specialized software packages. For the present research, the stochastic approach was implemented using AutoDock Vina, which utilizes a genetic algorithm for its search function (Ferreira *et al*., 2015). By modeling these interactions, docking provides critical insights into ligand behavior in the binding pocket and helps elucidate underlying biochemical mechanisms.

1.1.9.5 AUTODOCK VINA

AutoDock Vina (Vina) is one of the docking programs in the AutoDock Suite, together with AutoDock4 (AD4), AutoDock-GPU, AutoDockFR, and AutoDock-CrankPep.Vina is often regarded as one of the most popular programs, likely due to its user-friendly interface and fast performance, especially when compared to other docking software in the suite and beyond, as well as its open-source nature. Moreover, it supports the AutoDock4.2 scoring function, simultaneous docking of multiple ligands, and a batch mode for docking a large number of ligands. Furthermore, it implements Python bindings to facilitate scripting and the development of docking workflows. (Eberhardt *et al*., 2021)

1.1.10 THE VIRTUAL SCREENING PATHWAY

1.1.10.1 Target and Ligand Retrieval

The foremost step is to retrieve the specified molecular target, i.e, the target protein, from an appropriate database such as the RCSB Protein Data Bank (https://www.rcsb.org/). If the experimental structures of the target protein are unavailable, homology modeling can be used, which involves building protein 3D structures using protein primary sequence and utilizing prior knowledge gained from structural similarities with other proteins.(Hameduh *et al*., 2020) .It can

be done using servers such as SWISS-MODEL (https://swissmodel.expasy.org/) . The ligands under experimentation are also retrieved from an appropriate database, such as PubChem in standard file format and reduced in size by applying several molecular filters to preselect the drug-like molecules.

1.1.10.2 Target Preparation

Considering that the Target protein cannot be used as is, it is imperative that it be properly prepared to ensure that it is compatible with the docking software to be used. The retrieved protein structure is protonated and relaxed to avoid any steric clashes. The cocrystallized water molecules are also deleted.(Meng *et al*., 2011)

1.1.10.3 Binding Site Prediction

Protein-ligand docking aims to computationally forecast the precise three-dimensional position and orientation—known as the binding pose—of a small molecule ligand within its protein receptor. The location for this interaction, the binding pocket, can be defined beforehand using resources like the PLIP web server, which analyzes a protein's co-crystallized ligand, or it can be discovered through post-docking analysis. This fundamental distinction in methodology gives rise to two primary docking strategies:

Site-Directed Docking: This method is applied when the target binding site on the protein is known. The computational search is confined to a defined region around this site, which focuses the algorithm on sampling the ligand's translational, rotational, and conformational space efficiently. This targeted approach is standard in lead optimization, where understanding the precise binding mode is crucial for the rational design of analogs with enhanced potency and selectivity (Ghersi and Sanchez, 2009).

Blind Docking: This strategy is employed when the binding site is unknown, requiring the ligand to be docked across the entire solvent-accessible surface of the protein. The search space for blind docking is consequently much larger, encompassing the whole protein. To adequately explore this vast area, the number of computational evaluations must be significantly increased, which results in a proportionally longer simulation runtime.(Ghersi and Sanchez, 2009)

1.1.10.4 Protein-Ligand Docking

The primary outputs of a molecular docking simulation are the predicted three-dimensional pose of the ligand within the protein's binding site and an estimated binding free energy. To manage the computational complexity of this task, most docking software employs two key strategies. The first involves simplifying the system by constraining specific degrees of freedom, commonly treating the protein receptor as rigid and fixing the ligand's internal bond angles and lengths. The second strategy utilizes a simplified scoring function, frequently derived from empirical binding energy data, to enable the rapid evaluation of millions of potential ligand poses generated during the conformational search. (Forli *et al*., 2016)

1.1.10.5 Post-Docking Analysis

Molecular docking predicts both a ligand's binding pose and a score estimating binding affinity. However, the correlation between the best-scoring and most physically realistic pose is often imperfect. Therefore, docking scores should be considered provisional and must be validated through 3D visualization to accurately rank ligands (Sharma *et al*., 2021). This critical visual inspection verifies essential intermolecular interactions like hydrogen bonds and hydrophobic contacts.

1.1.11 ADMET PREDICTION

ADMET represents absorption, distribution, metabolism, excretion, and toxicity. These are essential processes and phenomena that take place. During the drug discovery process, the chemical synthesis aims for potent compounds with suitable physicochemical and ADMET characteristics that enable the drug to achieve an effective concentration at its target site. ADME modeling and calculations play a vital role in the development of new medications and in assessing the risks and side effects of substances that may come into contact with or enter the human body. The use of commercial software for the prediction of chemical and ADMET properties is convenient, since such tools can be used with virtual compounds and do not require any user data, while measured data are needed for local model building. (Borole and Khadse, 2024). Several commercial software types or online prediction tools are available for ADME and Toxicity prediction. They include Swiss ADME and Pro-Tox, which were used in this study, as well as ADMElab

1.1.12 DRUG LIKENESS

‘Drug-likeness’, A qualitative characteristic of potential therapeutic molecules determined by a vote from an expert committee or a set of rules integrated into software, in this case, is extensively incorporated into the initial phases of lead and drug discovery. Its conceptual development mainly progressed alongside research pertaining to Pfizer's 'rule of five' and lead-likeness, therefore situating it within this context. The discrimination between ‘drugs’ (represented by a collection of pharmaceutically relevant small molecules, some of which are marketed drugs) and ‘nondrugs’ (typically, chemical reagents) is possible using a wide variety of statistical tools and chemical descriptor systems (Ursu *et al*., 2011)

1.1.12.1 LIPPINSKI RULE OF FIVE

Lipinski's ‘rule of five’ is the first qualitative attempt to guide the design of ‘orally deliverable’ compounds and is based on the limits on properties (clogP, molecular weight, and number of hydrogen-bond donors and acceptors) beyond which oral activity is predicted to be poor (Pillai *et al*., 2001)

In the discovery setting, `the rule of 5' predicts that poor absorption or permeation is more likely when there are more than 5 H-bond donors, 10 H-bond acceptors, the molecular weight (MWT) is greater than 500, and the calculated Log P (CLogP) is greater than 5 (or MlogP>4.15). Note that all numbers are multiples of five, which is the origin of the rule's name. It is also important to note that the Rule of 5 only holds for compounds that are not substrates for active transporters. (Lippinski *et al*., 2001)

1.1.12.2 VARIANTS AND EXTENSIONS

The discovery of various protein/receptor targets from genomic research is expanding rapidly. Along with the automation of organic synthesis and biochemical screening, this is bringing a major change in the whole field of drug discovery research, thus requiring an improvement in the major criteria used to determine drug-likeness. One major example of this variant/ improvement done on the Rule of Five is the Ghose filter, and its criteria are detailed as follows:

- Partition coefficient log *P* in −0.4 to +5.6 range
- Molar refractivity from 40 to 130 with an average value of 97
- Molecular weight from 180 to 480

- Total number of atoms from 20 to 70 (includes H-bond donors [e.g., OHs and NHs] and H-bond acceptors [e.g., Ns and Os]) with an average value of 48.

The objective of this work was to provide both quantitative and qualitative characterization of known drugs, which would help in generating 'drug-like' libraries, thus enabling researchers to use resources efficiently when searching for lead compounds. (Ghose *et al*.,1999)

Another extension, Veber's rule, suggests that the commonly applied molecular weight cutoff at 500 does not itself significantly separate compounds with poor oral bioavailability from those with acceptable values, and instead states that compounds which meet only the two criteria of:

- 10 or fewer rotatable bonds and,
- Polar surface area equal to or less than 140 Å2 (or 12 or fewer H-bond donors and acceptors) will have a high probability of good oral bioavailability.

It also suggests that reduced polar surface area correlates better with increased permeation rate than does lipophilicity (C log P), and increased rotatable bond count has a negative effect on the permeation rate. A threshold permeation rate is a prerequisite of oral bioavailability. (Veber *et al*., 2002)

These extensions could also be considered when determining molecules that are 'drug-like.'

1.1.13 LEAD OPTIMIZATION

The drug discovery process culminates in a phase dedicated to molecular refinement, where the core objective is a dual-purpose structural enhancement. This stage, known as lead optimization, focuses on amplifying a compound's therapeutic potential while systematically eliminating its molecular flaws. Strategies for these improvements are dual-sourced, derived either from empirical data from techniques like mass spectrometry or from computational predictions. The latter leverages powerful in silico tools such as molecular dynamics, QSAR, pharmacophore modeling, and docking simulations to guide the chemical redesign. (Barcelos *et al*, 2022)

1.1.14 AIM OF THE STUDY

The objectives of this study are stated below :

- Investigate and compare the antiviral potential of Artemisia annua compounds (Isolated and GC-MS derived) against SARS-CoV-2 helicase (5RMM).
- Use molecular docking and ADMET profiling to identify promising drug candidates.
- Highlight phytoconstituents with strong binding affinity and favorable pharmacokinetics.
- Support natural product-based drug discovery for COVID-19 treatment.

1.1.15 JUSTIFICATION OF THE STUDY

The persistent global threat posed by SARS-CoV-2, coupled with the limitations of existing therapeutics, necessitates the exploration of novel antiviral agents. Targeting the highly conserved helicase protein 5RMM offers a promising strategy for broad-spectrum inhibition across coronaviruses. Artemisia annua, a medicinal plant with documented antiviral properties, presents a viable source of bioactive compounds. This study employs computational methods to evaluate the inhibitory potential of its phytoconstituents, aiming to identify safe, effective, and accessible candidates for COVID-19 treatment.

CHAPTER TWO

2.1 MATERIALS AND METHODS

2.1.1 PUBCHEM

PubChem is a publicly accessible resource for chemical information, created and maintained by the National Center for Biotechnology Information (NCBI) at the National Library of Medicine (NLM), which is part of the U.S. National Institutes of Health (NIH). It gathers descriptions of chemical substances and their biological activities from over 500 data sources and makes this information available to the public (Kim, 2019). The information in PubChem is structured into three interconnected databases: Substance (with more than 286 million substance descriptions as of this writing), Compound (featuring over 111 million unique chemical structures), and BioAssay (which includes 1.2 million biological assays related to more than 10,000 target protein sequences).(Stanzione *et al*., 2021)

2.1.2 RCSB PDB

The Protein Data Bank (PDB; http://www.rcsb.org/pdb/) is the sole global repository for structural information on biological macromolecules. Established in 1971 at Brookhaven National Laboratories, the PDB originally served as a database for macromolecular crystal structures, starting with just seven entries. The pace of growth increased during the 1980s due to advancements in crystallography, the addition of NMR-derived structures, and a move towards open data sharing. In October 1998, the Research Collaboratory for Structural Bioinformatics (RCSB) took over the management of the PDB. Once primarily accessible to structural biology specialists, the PDB now supports a wide range of users, including those in biology, chemistry, computer science, educators, and students. Contributors to the PDB include experts in crystallography, NMR, cryo-EM, and theoretical modeling.(Berman *et al*., 2000)

2.1.3 PyRx

PyRx (Python Prescription) is a flexible Virtual Screening tool intended for Computational Drug Discovery. It allows Medicinal Chemists to perform Virtual Screening from any platform by screening compound libraries against possible drug targets. PyRx makes the entire process more efficient, encompassing everything from data preparation to job submission and analysis of results. Virtual screening (VS) is a computational approach used to examine large databases of molecules to identify potential lead compounds. Docking-based virtual screening (DBVS) techniques explore the interactions between small molecules and the binding sites of target proteins, enabling the selection of compounds that demonstrate the best binding properties for subsequent experimental validation. The main characteristics consist of a user-friendly graphical interface, smooth compatibility with Auto Dock 4.2 and Auto Dock Vina for accurate predictions of ligand-target binding affinities, and sophisticated features for comprehensive library screening and result analysis. PyRx additionally facilitates energy docking simulations, molecular structure minimization, and provides cross-platform support (Windows, macOS, Linux), guaranteeing wide accessibility. (Kannan *et al*., 2025)

2.1.4 PLIP

PLIP, which stands for protein–ligand interaction profiler, examines molecular interactions within protein structures. It identifies eight different categories of non-covalent interactions. Originally concentrated on interactions between small molecules, DNA, and RNA with proteins, the latest version now includes protein–protein interactions. PLIP demonstrates how a drug can mimic the native interaction, as there is significant overlap in the interaction profiles. It has found extensive application in three primary areas: drug screening workflows, characterization of protein complexes, and deep learning. (Schake *et al*., 2025). In this study, it was used to determine the binding site amino acid residues of the protein, 5RMM.

2.1.5 Biovia Discovery Studio 2025

Discovery Studio is a collection of software designed for simulating systems involving small molecules and macromolecules. It serves applications in molecular modeling, simulation, and data analysis across life sciences, materials science, and chemistry, enhancing the drug discovery process with tools for structure-based and ligand-based design, as well as molecular simulations. This software aids researchers in refining therapeutic candidates from the stage of target identification to lead optimization. (Dassault Systèmes, 2025). This software plays a crucial role in the analysis that follows docking. This study utilized version 25.1.0.24284, which was released in 2025.

2.1.6 SwissADME

SwissADME is a web tool that gives free access to a pool of fast yet robust predictive models for the analysis and determination of the physicochemical properties, pharmacokinetics, drug-likeness, and medicinal chemistry friendliness of ligand molecules, among which are in-house proficient methods such as the BOILED-Egg, iLOGP, and Bioavailability Radar, thus enabling researchers to evaluate the safety and potential efficacy of new compounds under inspection. (Daina *et al*., 2017)

2.1.7 ProTox-3.0

Toxicity evaluation is one of the main steps in drug and chemical design. Hence, there is a high demand for computational predictive models to evaluate the potential toxic effects of drugs and chemicals. ProTox 3.0 is a web tool that incorporates molecular similarity and machine-learning models for the prediction of 61 toxicity endpoints, such as acute toxicity, organ toxicity, clinical toxicity, molecular-initiating events (MOE), adverse outcomes (Tox21) pathways, several other toxicological endpoints, and toxicity off-targets. (Banerjee *et al*., 2024). In this study, version 3.0 of the platform, the latest update, was used.

2.1.8 COMPUTER SYSTEM

The in-silico study was conducted using a laptop with the following specifications :

Model: HP EliteBook 1050 G1

Processor: Intel® Core™ i7-8850H CPU @ 2.60 GHz

RAM: 32.00 GB

ROM: 477 GB

System type: 64-bit Operating system, x64-based processor

Operating system: Windows 11 Pro

2.2 METHOD

2.2.1 COLLECTION AND EXTRACTION OF THE PLANT MATERIALS (ISOLATED COMPOUNDS)

The isolated compounds of the plant Artemisia annua were obtained from the literature (Anibogwu *et al*., 2021)

2.2.2 PLANT COLLECTION AND PREPARATION

The plant collection and identification are detailed in the table below :

Table 2.1: Plant Collection and Identification

S/N	Plant name	Plant	Place of	Date of	Plant ID

		part	collection	collection	
1	Artemisia annua	Leaves	Ibafo, Ogun State	April, 2021	FHI113652

*FHI = Forestry Research Institute of Nigeria, Ibadan, Voucher number.

2.2.2.1 PLANT PREPARATION AND EXTRACTION

The plant materials (leaves, Table 1) were air-dried for 3 weeks, ground into powder, and stored in an air-tight container until ready. The powdered plant materials (200 g each) were extracted separately by maceration in methanol (2 L) at room temperature for 1 week. The extracts were concentrated *in vacuo* using a rotary evaporator at 45℃ and then stored in a refrigerator at 4℃ until further use.

2.2.3 GC-MS EXTRACTION

A gas chromatograph manufactured by Agilent USA, hyphenated with a mass spectrophotometer (5975C) featuring a triple axis detector and equipped with an auto injector using a 10 µL syringe, was utilized. Helium acted as the carrier gas throughout the process. All chromatographic separations were conducted on a capillary column with the following specifications: a length of 30 m, an internal diameter of 0.2 µm, and a thickness of 250 µm, treated with phenyl methyl siloxane. The other GC-MS conditions included an ion source temperature of 250℃ (EI), an interface temperature of 300℃, a pressure of 16.2 psia, an out time of 1.8 mm, and a 1 µL injection in Split mode with a split ratio of 1:50, with the injection temperature set to 280℃. The column temperature commenced at 50℃ for 2 minutes and was increased to 100℃ at a rate of 20℃ per minute. It was then raised to 250℃ at the same rate and maintained for an additional 5 minutes, resulting in a total elution time of 19 minutes. The MS Solution software provided by the manufacturer was utilized to manage the system and collect data; the identification of compounds was performed by comparing the obtained mass spectra with standard mass spectra from the NIST library (NISTII).

Machine model: 7890A GC system, 5675C Inert MSD with triple–axis detector

Packing material: Capillary column

Carrier gas: Helium gas

Flow rate: in the instrumentation parameter

Column length: 30m

Dimension: 30mx250umx 0.25um

Column: Agilent 19091- 433HP-5Ms 5% phenyl methyl silox

2.2.4 PREPARATION OF PROTEIN TARGET

The protein target, 5RMM, was retrieved from the Protein Data Bank (PDB) (https://rcsb.org). It was prepared using Biovia Discovery Studio 2025, removing water molecules, heteroatoms, non-standard residues, and unnecessary protein side chains not required for docking, while adding polar hydrogens. The prepared protein was saved in the PDB format. Before docking, the protein was loaded into PyRx and converted to an Autodock macromolecule.

2.2.5 IDENTIFICATION OF THE BINDING SITE

The active or binding site amino acids were identified using the Protein–Ligand Interaction Profiler (PLIP), which analyzed the co-crystallized protein–ligand complex and detailed the specific amino acids involved in ligand binding. Analysis of the website revealed ASP 534, ASN 177, ASN 516, and ARG 560 as the pertinent amino acid residues at the protein-binding site.

2.2.6 IDENTIFICATION AND PREPARATION OF LIGANDS

The Open Babel plug-in was used to import the SDF files of the phytochemicals isolated from the plant Artemisia annua, as well as those obtained via GC-MS extraction, into PyRx. The SDF files were obtained from PubChem and prepared for docking via minimization and conversion to AutoDock ligands (pdbqt).

2.2.7 MOLECULAR DOCKING

The prepared protein target was loaded into PyRx and converted into a macromolecule; all ligands were imported into PyRx in SDF format. To ensure accurate docking, a grid box was defined around the labeled binding site amino acids, serving as a spatial guide for the AutoDock Vina plugin. The dimensions of the grid box were X: 28.2731 Å, Y: 18.3412 Å, and Z: 23.1176 Å.

Docking was carried out at an exhaustiveness of 5. Upon completion of docking, the binding affinities were obtained for all ligands and saved as Comma-Separated Values (CSV).

2.2.8 POST DOCKING ANALYSIS

The ligands with a binding affinity ≤ -7 kcal/mol and ≤ -6.5 kcal/mol were selected for receptor-ligand interactions for the Isolated compounds and GC-MS extracts of *Artemisia annua*, respectively. The various binding conformations of each ligand against the protein were saved from PyRx in the PDB format. The interactions between the identified binding site amino acid residues and the ligands were then analysed using Biovia Discovery Studio Visualizer 2025. The 3D and 2D analyses were done to visualise the various binding models of each ligand and determine the ligands with higher potential for antiviral activity.

2.2.9 ADMET PROFILING

The selected compounds were subjected to ADMET analysis to evaluate their pharmacokinetic and toxicity profiles. The absorption, distribution, metabolism, excretion, and toxicity (ADMET) properties of the test ligands, including physicochemical parameters and toxicity-related pharmacokinetic characteristics, were assessed using in silico integrative tools such as the SwissADME platform and the ProTox v3.0 webserver.

CHAPTER THREE

RESULTS

The results of the *in-silico* analysis of the isolated compounds and the GC-MS derived compounds of *Artemisia annua* are presented below:

3.1 GC-MS EXTRACTION

The table below presents the GC-MS data for n-hexane-derived compounds from *Artemisia annua.*

Table 3.1. GC-MS of n-hexane-derived compounds of *Artemisia annua*

S/N	COMPOUNDS	PUBCHEM CID	MOL. FORMUL	MOL. WEIGHT	RETENTION TIME	AREA %

			A			
1	Undecane	14257	$C_{11}H_{24}$	156.31 g/mol	5.033	6.58
2	Benzoic acid, methyl ester	7150	$C_8H_8O_2$	136.15 g/mol	5.164	19.14
3	Methyl 4-methylvalerate	17008	$C_7H_{14}O_2$	130.18 g/mol	5.456	4.43
4	Oct-3-ene-1,5-diyne, 3-t-butyl-7,7 -dimethyl	5362777	$C_{14}H_{20}$	188.31 g/mol	9.988	7.6
5	3,5-Di-tert-butylphenol	70825	$C_{14}H_{22}O$	206.32 g/mol	10.165	4.35
6	5,6,7,8-Tetramethyl-1,2,3,4-tetrahydronaphthalene	599685	$C_{14}H_{20}$	188.31 g/mol	10.469	12.2
7	1,6-Ethenoazulene, 1,3a,6,8a-tetrahydro-	562313	$C_{12}H_{12}$	156.22 g/mol	10.766	5.53
8	1,8-Cyclopentadecadiyne	138329	$C_{15}H_{22}$	202.33 g/mol	10.909	5.87
9	Pyrethrone	5373801	$C_{11}H_{14}O$	162.23 g/mol	12.477	5.36
10	Pinane	10129	$C_{10}H_{18}$	138.25 g/mol	13.238	69.53
11	5-methylspiro [3.5]-nonan-1-one	557033	$C_{10}H_{16}O$	152.23 g/mol	13.461	6.67
12	3,4-Octadiene, 7-methyl-	142131	C_9H_{16}	124.22 g/mol	13.627	17.67
13	Methyl hexadecanoate	8181	$C_{17}H_{34}O_2$	270.5 g/mol	14.045	61.44
14	(E)-Ligustilide	5877292	$C_{12}H_{14}O_2$	190.24 g/mol	14.165	7.85
15	n-Hexadecanoic acid	985	$C_{16}H_{32}O_2$	256.42 g/mol	14.457	39.21
16	Bicyclo[3.3.1]nonan-9-ol, 9-methyl-	543604	$C_{10}H_{18}O$	154.25 g/mol	14.583	10.56
17	5-Octadecenal	545652	$C_{18}H_{34}O$	266.5 g/mol	14.657	4.16
18	2-Methyl-Z,Z-3,13-octadecadienol	5364412	$C_{19}H_{36}O$	280.5 g/mol	14.863	4.4
19	4-Isopropenyl-4,7-dimethyl-1-oxaspiro[2.5]octane	543441	$C_{12}H_{20}O$	180.29 g/mol	15.029	15.25
20	Deoxyartemisinin	12814879	$C_{15}H_{22}O_4$	266.33 g/mol	15.252	80.45
21	Methyl linolelaidate	5362793	$C_{19}H_{34}O_2$	294.5 g/mol	15.453	19.06

22	Methyl cis-9-octadecenoate	5364509	$C_{19}H_{36}O_2$	296.5 g/mol	15.504	38.62
23	Cyclododecanone, 2-methylene-	534631	$C_{13}H_{22}O$	194.31 g/mol	15.556	11.57
24	1,2-15,16-Diepoxyhexadecane	543423	$C_{16}H_{30}O_2$	254.41 g/mol	15.601	25.39
25	Methyl stearate	8201	$C_{19}H_{38}O_2$		15.727	18.22
26	9,17-Octadecadienal, (Z)-	5365667	$C_{18}H_{32}O$	264.4 g/mol	15.95	100
27	9-Hexadecenoic acid	4668	$C_{16}H_{30}O_2$	254.41 g/mol	16.168	25.57

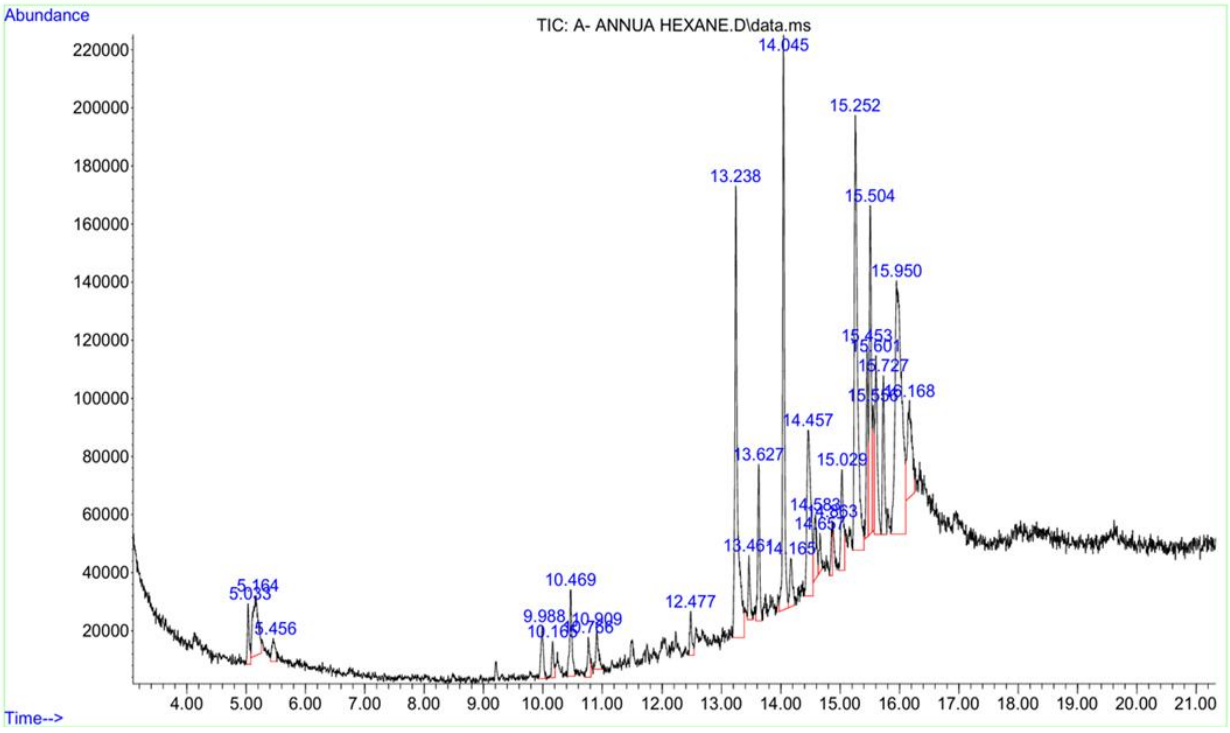

Figure 3.1: The GC-MS chromatogram for the n-Hexane extraction of *Artemisia annua*

S/N	COMPOUNDS	PUBCHEM CID	MOL. FORMULA	MOL.WEIGHT	RETENTION TIME	AREA %
1	Hept-2-yne	14245	C_7H_{12}	96.17 g/mol	3.139	5.32
2	Undecane	14257	$C_{11}H_{24}$	156.31 g/mol	5.033	9.05
3	Octadecyl pentadecafluorooctanoate	15918848	$C_{26}H_{37}F_{15}O_2$	666.5 g/mol	5.124	11.3
4	Methylbenzoate	7150	$C_8H_8O_2$	136.15 g/mol	5.164	21.08
5	Methyl octanoate	8091	$C_9H_{18}O_2$	158.24 g/mol	5.45	6.46
6	2-methoxy-5,6-dimethylpyridine-3,4-dicarbonitrile	46949601	$C_{10}H_9N_3O$	187.20 g/mol	10.909	5.25
7	3H-Cyclodeca[b]furan-2-one, 4,9-dihydroxy-6-methyl-3,10-dimethylene-3a,4,7,8,9,10,11,11a-octahydro-	6110227	$C_{15}H_{20}O_4$	264.32 g/mol	13.238	5.38
8	Glyceryl diacetate 2-oleate	5363238	$C_{25}H_{44}O_6$	440.6 g/mol	13.736	4.46
9	Methyl hexadecanoate	8181	$C_{17}H_{34}O_2$	270.5 g/mol	14.045	35.69
10	Hexadecanoic acid	985	$C_{16}H_{32}O_2$	256.42 g/mol	14.457	39.77
11	Civetone	5315941	$C_{17}H_{30}O$	250.4 g/mol	15.149	6.13
12	Germacrene D-4-ol	5352847	$C_{15}H_{26}O$	222.37 g/mol	15.269	14.89
13	2-Methyl-Z,Z-3,13-octadecadienol	5364412	$C_{19}H_{36}O$	280.5 g/mol	15.458	8.81
14	Methyl petroselinate	5362717	$C_{19}H_{36}O_2$	296.5 g/mol	15.504	25.67
15	12-Methyl-E,E-2,13-octadecadien-1-ol	90107969	$C_{19}H_{36}O$	280.5 g/mol	15.567	18.7
16	Methyl octadecanoate	8201	$C_{19}H_{38}O_2$	298.5 g/mol	15.721	18.4
17	10-Methyl-E-11-tridece-1-ol acetate	5363277	$C_{16}H_{30}O_2$	254.41 g/mol	15.79	4.12
18	(Z)-14-Methylhexadec-8-enal	5364688	$C_{17}H_{32}O$	252.4 g/mol	15.95	100
19	(Z)-Tetradec-7-enal	5364468	$C_{14}H_{26}O$	210.36 g/mol	16.111	5.88
20	oleic acid	445639	$C_{18}H_{34}O_2$	282.5 g/mol	16.156	26.34
21	7-Pentadecyne	549063	$C_{15}H_{28}$	208.38 g/mol	16.585	17.7
22	2(1H)-Naphthalenone, octahydro-4a-methyl-7-(1-methylethyl)-. (4aalpha,7beta,8abeta)-	41133	$C_{14}H_{24}O$	208.34 g/mol	16.923	38.66
23	8-Oxabicyclo(5.1.0)octane	67512	$C_7H_{12}O$	112.17 g/mol	17.724	4

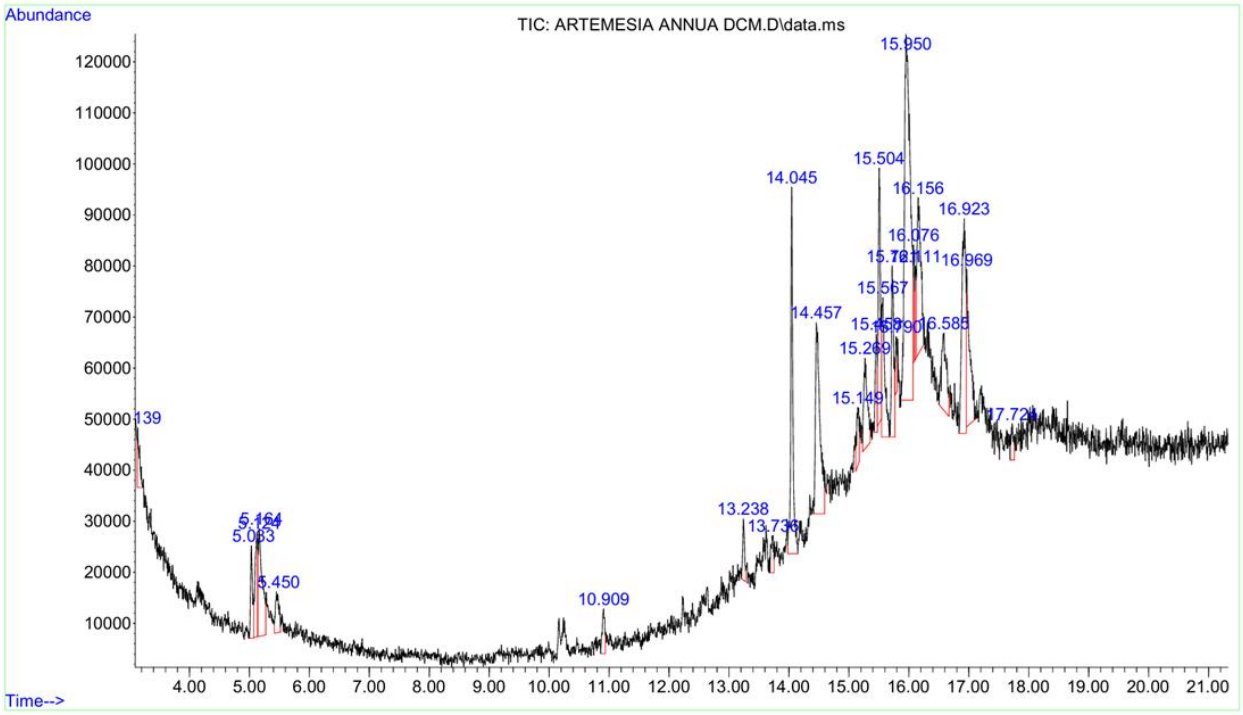

Figure 3.2: The GC-MS chromatogram for the Dichloromethane extraction of *Artemisia annua*

3.2 BINDING AFFINITIES

3.2.1 Binding Site Amino acids of 5RMM

The result of the binding site amino acids identified using PLIP is shown in Table 3.3

Table 3.3: Binding site amino acids of the protein 5RMM

S/N	BINDING SITE AMINO ACIDS
1	ASP 534
2	ASN 177
3	ASN 516
4	ARG 560

3.2.2 MOLECULAR DOCKING

The molecular docking analysis results of the isolated compounds and GC-MS extracts of *Artemisia annua,* the co-crystallized ligand, and the standard antiviral drug, Nilotinib, show that the compounds exhibited varying degrees of binding affinities with the non-structural target protein, 5RMM.

Table 3.4. Binding affinities of isolated *Artemisia annua* compounds

S/N	NAME OF COMPOUND	PUBCHEM CID	BINDING AFFINITY (Kcal/mol)
1	Cirsiliol	160237	-7.9
2	Cirsilineol	162464	-7.5
3	Cirsimartin	188323	-7.2
4	Chlorogenic acid	1794427	-7.9
5	Acacetin	5280442	-7.4
6	Apigenin	5280443	-7.3
7	Luteolin	5280445	-7.8
8	Chrysoeriol	5280666	-7.5
9	Kaempferol	5280863	-7.3
10	Axillarin	5281603	-7.7
11	Isorhamnetin	5281654	-7.5
12	Rhamnetin	5281691	-9.3
13	Astragalin	5282102	-8.7

14	Quercimeritrin	5282160	-9.5
15	Casticin	5315263	-7.5
16	Artemetin	5320351	-7.6
17	Retusin	5352005	-7.3
18	Eupatorin	97214	-7.5

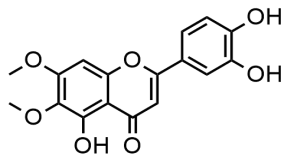

Cirsiliol

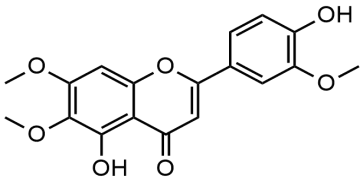

Cirsilineol

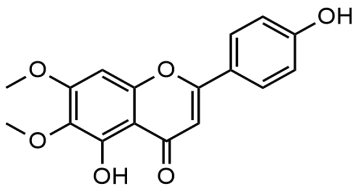

Cirsimaritin

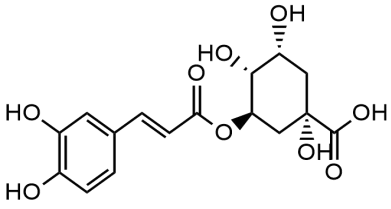

chlorogenic acid

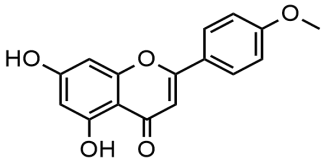

acacetin

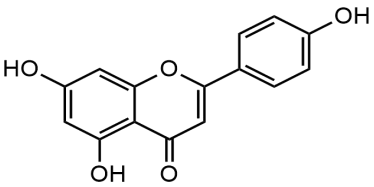

apigenin

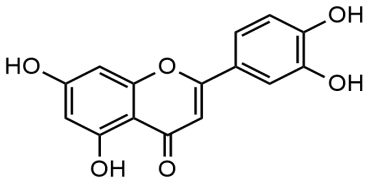

luteolin

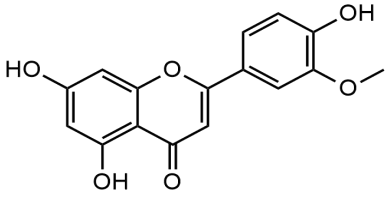

Chrysoeriol

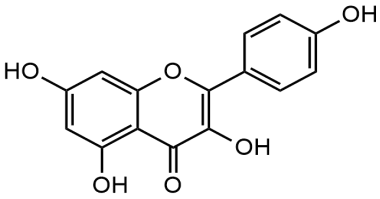

kaempferol

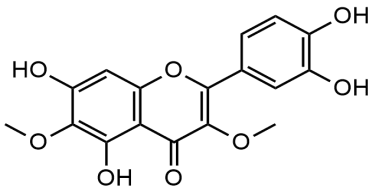

Axillarin

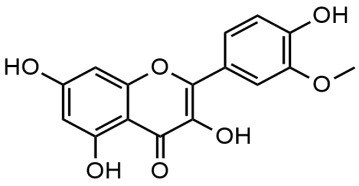

Isorhamnetin

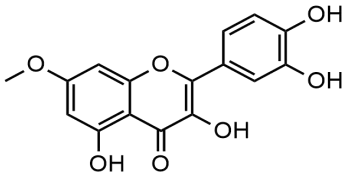

Rhamnetin

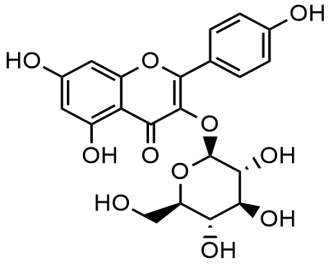

Astragalin

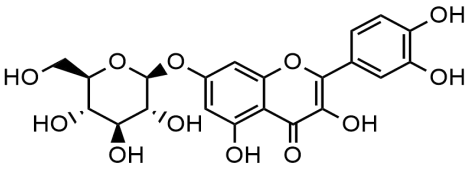

Quercimeritrin

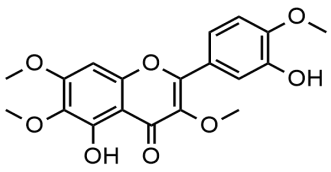

Casticin

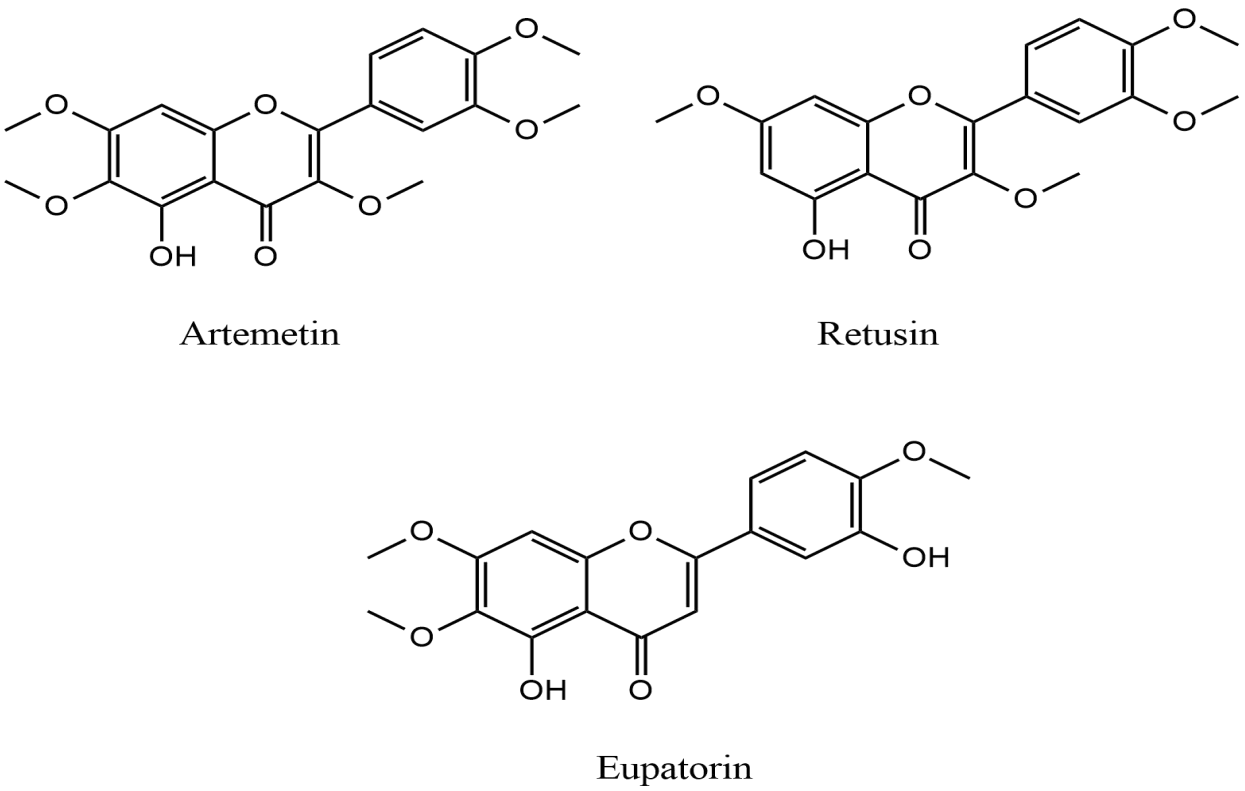

Figure. 3.3 Isolated compounds of *Artemisia annua*

Table 3.5 Binding affinities of GC-MS Hexane Extract of *Artemisia annua* compounds.

S/N	NAME OF COMPOUNDS	PUBCHEM CID	BINDING AFFINITY (Kcal/mol)
1	1,8-Cyclopentadecadiyne	138329	-6.7
2	Cyclododecanone, 2-methylene-	534631	-6.6
3	Deoxyartemisinin	12814879	-7.8

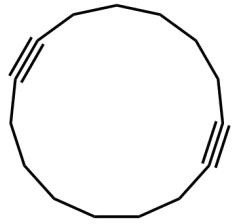

1,8-Cyclopentadecadiyne

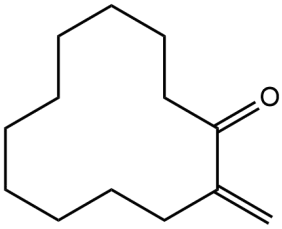

Cyclododecanone, 2-methylene-

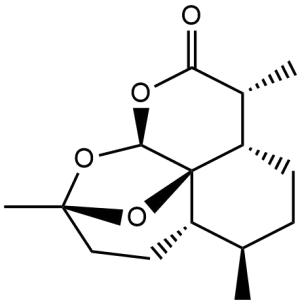

Deoxyartemisinin

Figure 3.4. Compounds in GC-MS n-Hexane extract of *Artemisia annua*

Table 3.6. Binding affinities of GC-MS Dichloromethane Extract of *Artemisia annua* compounds.

S/N	NAME OF COMPOUNDS	PUBCHEM CID	BINDING AFFINITY (Kcal/mol)
1	2(1H)-Naphthalenone, octahydro-4a-methyl-7-(1-methylethyl)-. (4aalpha,7beta,8abeta)-	41133	-6.6
2	Civetone	5315941	-7.3
3	Germacrene D-4-ol	5352847	-6.9
4	3H-Cyclodeca[b]furan-2-one, 4,9-dihydroxy-6-methyl-3,10-dimethylene-3a,4,7,8,9,10,11,11a-octahydro-	6110227	-7.7

5	Octadecyl pentadecafluorooctanoate	15918848	-6.6

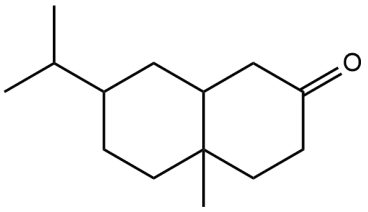

2(1H)-Naphthalenone, octahydro-4a-methyl-7-(1-methylethyl)-. (4aalpha,7beta,8abeta)-

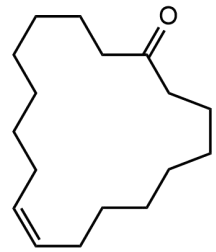

Civetone

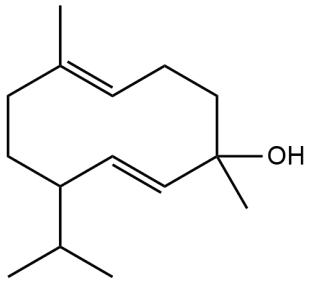

Germacrene D-4-ol

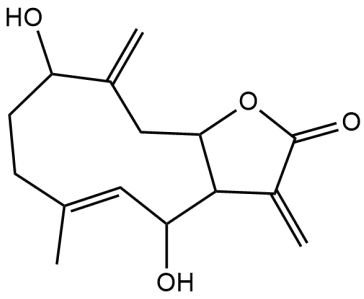

(5E)-4,9-dihydroxy-6-methyl-3,10-dimethylidene-4,7,8,9,11,11a-hexahydro-3aH-cyclodeca[b]furan-2-one

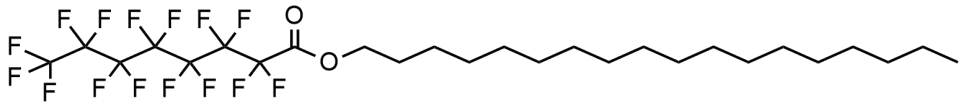

Octadecyl pentadecafluorooctanoate

Figure. 3.5. Compounds in GC-MS Dichloromethane extract of *Artemisia annua.*

Table 3.7. Binding affinities of Nilotinib and the Native Ligand (VXG) compounds

S/N	NAME OF COMPOUNDS	PUBCHEM CID	BINDING AFFINITY (Kcal/mol)
1	(3S,4R)-1-acetyl-4-phenylpyrrolidine-3-carboxylic acid (VXG)	155387694	-6.7
2	Nilotinib	644241	-10.1

Figure 3.6 The NSP-13 Helicase protein, 5RMM, with its co-crystallized ligand VXG.

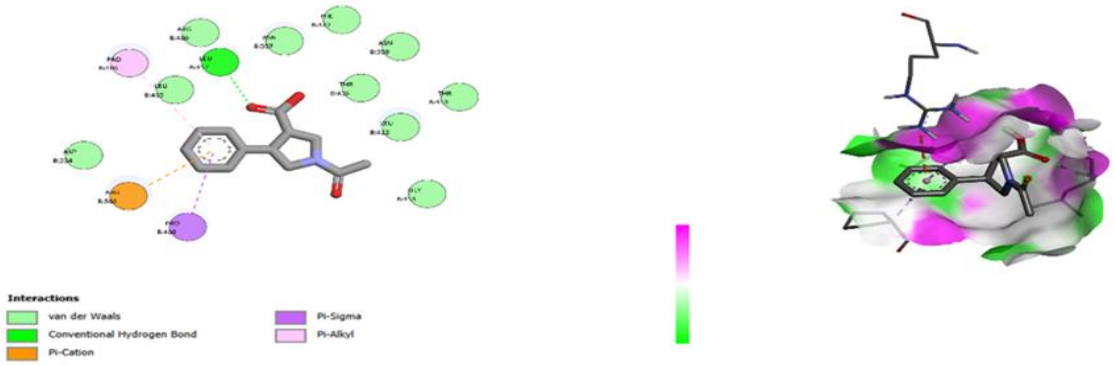

Figure 3.7: Ligand interaction schematic of the co-crystallized ligand VXG with the protein 5RMM.

3.3 2D and 3D ligand interactions of the phytoconstituents of *Artemisia annua* with 5RMM

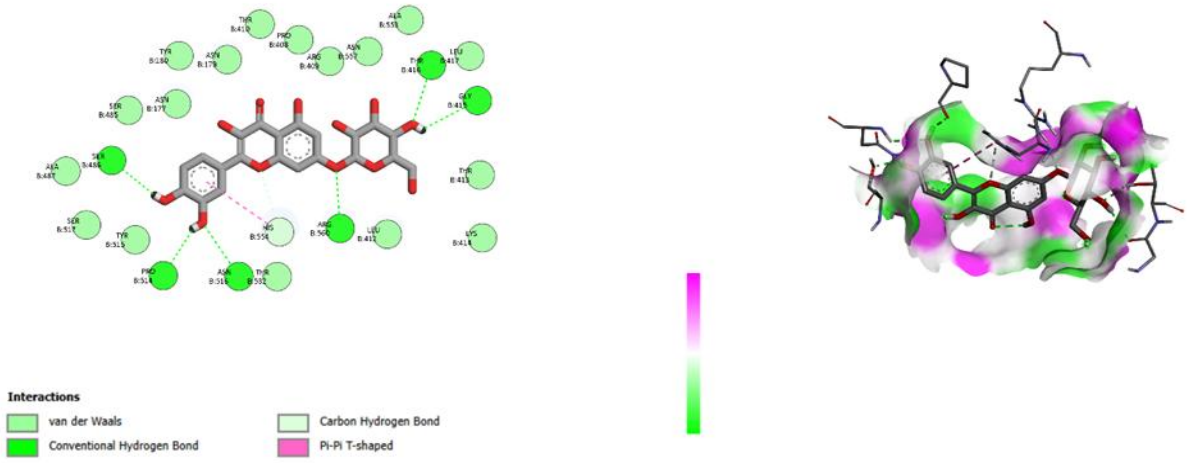

Figure 3.8: Ligand interaction schematic of the isolated compound Quercimeritrin with the protein 5RMM

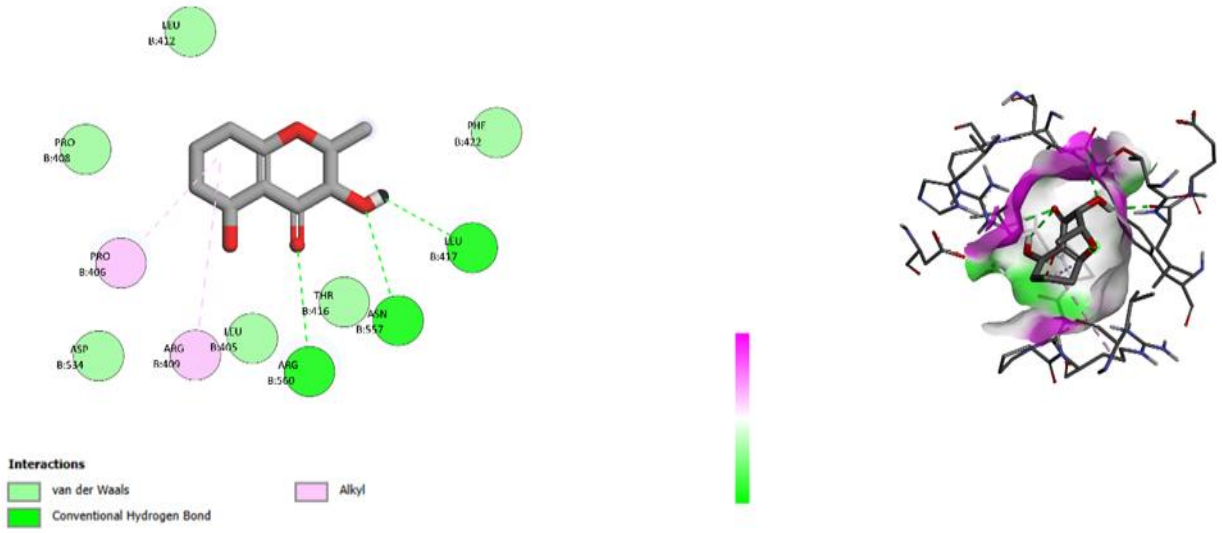

Figure 3.9: Ligand interaction schematic of the isolated compound Rhamnetin with the protein 5RMM

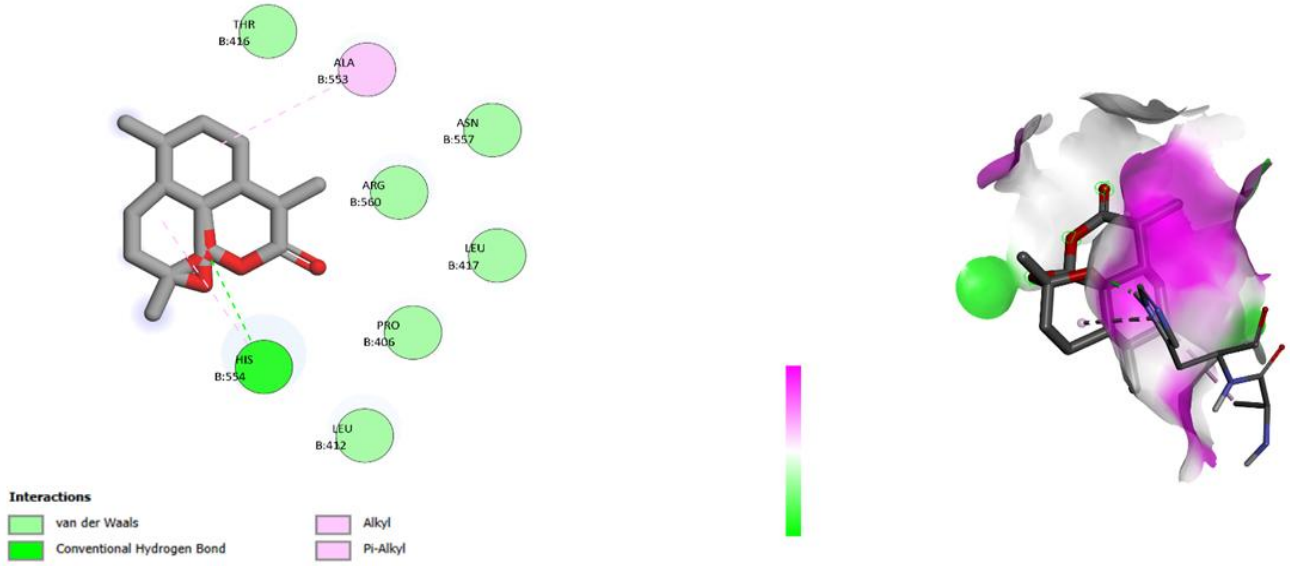

Figure 3.10: Ligand interaction schematic of the GC-MS n-Hexane derived compound Deoxyartemisinin with the protein 5RMM.

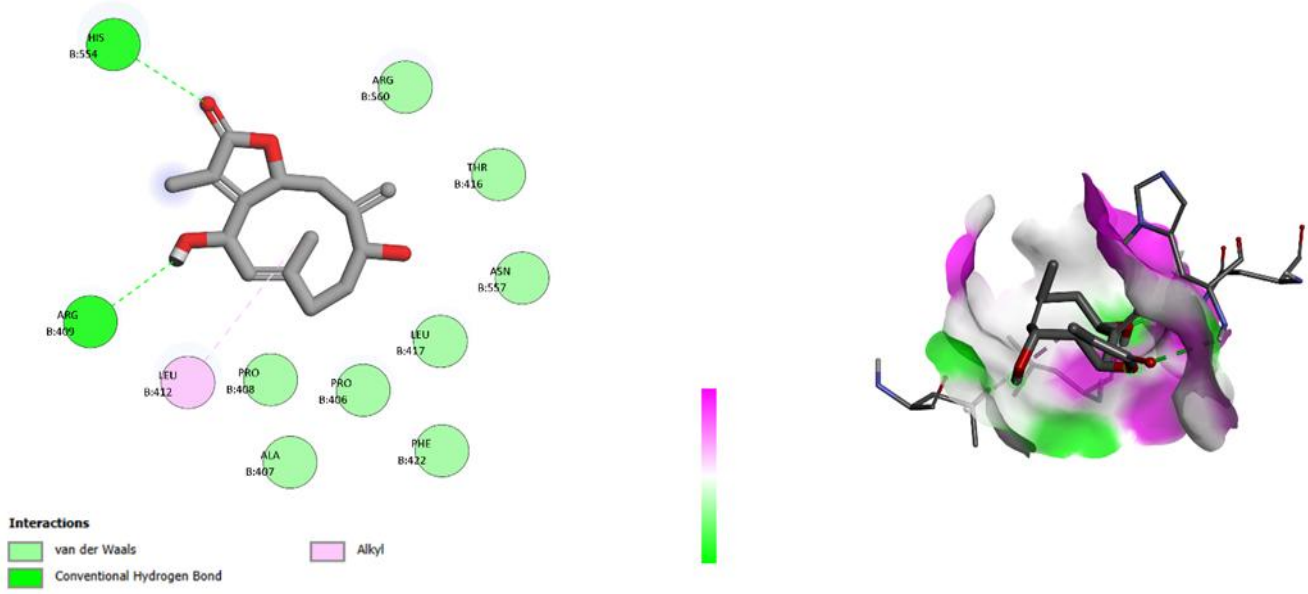

Figure 3.11: Ligand interaction schematic of the GC-MS Dichloromethane derived compound 3H-Cyclodeca[b]furan-2-one, 4,9-dihydroxy-6-methyl-3,10-dimethylene-3a,4,7,8,9,10,11,11a-octahydro- with the protein 5RMM.

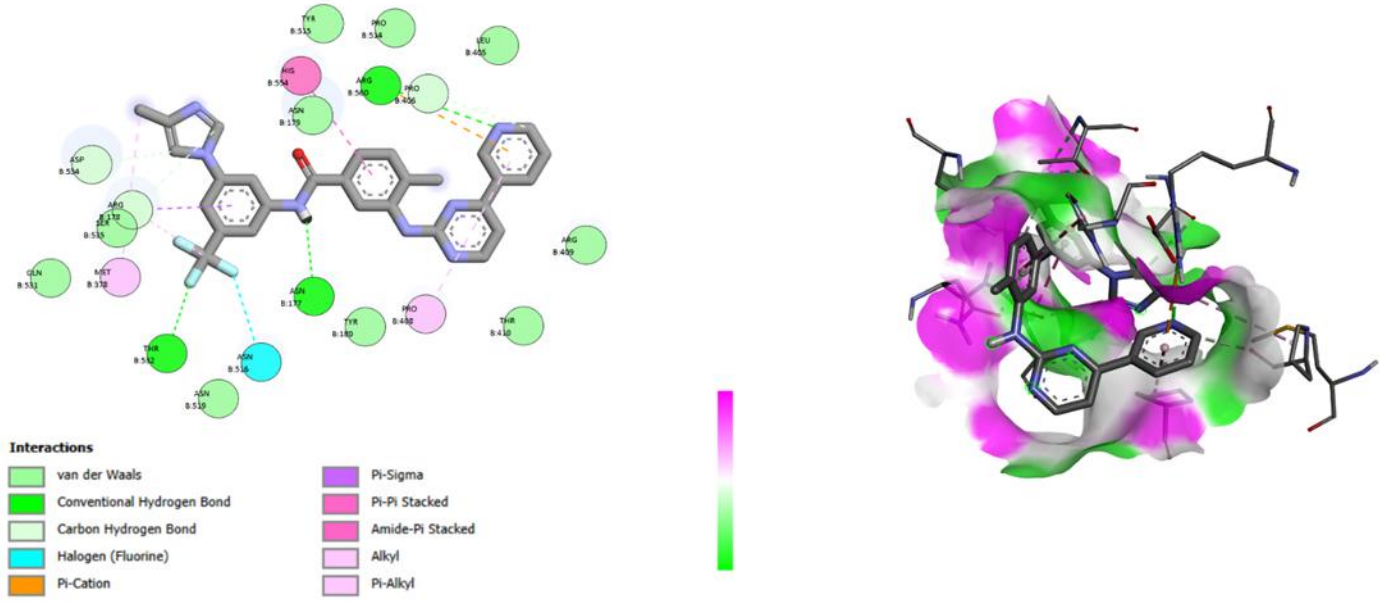

Figure 3.12: Ligand interaction schematic of the standard Nilotinib with the protein 5RMM

Table 3.8: Ligand (*Artemisia annua* isolated compounds) interaction with Amino acids on the target protein, 5RMM.

S/N	Ligands	HYDROGEN BOND	VAN DER WAALS FORCES	OTHERS
1	Cirsiliol	SER 486, PRO 514, ARG 409	ARG 560 , THR 532, TYR 515, ASN 516, SER 517, SER 485, ASN 177, ASN 179, THR 410, TYR 180, PRO 408, LEU 412	Carbon-hydrogen bond
2	Cirsilineol	SER 485, ASN 177, HIS 554, ARG 409	ASN 516, TYR 515, ALA 407, PRO 408, LEU 412, LEU 417, THR 416, ASN 557	Carbon-hydrogen bond, Pi-cation, Pi-Pi T-shaped, Alkyl, Pi-Alkyl
3	Cirsimaritin	LEU 412, ARG 409, ARG 560, ASN 557	ASN 559, PHE 422, PRO 419, THR 416, LEU 417, THR 410, ASN 177, PRO 408, LEU 405	Carbon-hydrogen bond Pi-Alkyl
4	Chlorogenic acid;	ARG 409, ASN 179, ASN 177	SER 485, TYR 180, PRO 175, THR 410, PRO 408, LEU 412, PHE 422, ASN 559, ASN 557, LEU 405, ARG 560, HIS 554	Pi-Alkyl
5	Acacetin	ARG 560, ASN 557	ASN 559, LEU 405, PHE 422, ASP 534, PRO 408, ASN 179, ASN 177, ASN 516, HIS 554, LEU 412, THR 416, LEU 417, GLY 415	Pi-Alkyl
6	Apigenin	ARG 560, ASN 179	PRO 408, TYR 180, THR 410, LEU 412, ARG 409, GLU 418, LEU 417, THR 416, ASN 557, PRO 419, PHE 422, LEU 405	Pi-Pi T-shaped, Pi-Alkyl
7	Luteolin	LEU 417	THR 416, PHE 422, LEU 412, THR 413, THR 410, TYR 180, PRO 408, ASN 179, ARG 560, LEU 405, ASN 559, ASN 557	Pi-Alkyl, Amide-Pi Stacked
8	Chrysoeriol	HIS 554, ARG 560, LEU 417	ALA 553, ASN 556, THR 416, PHE 422,	Pi-Cation, Pi-Alkyl

			ARG 409, THR 410, TYR 180, ASN 179, ASN 177	
9	Kaempferol	LEU 417, GLY 415, ASN 557	LEU 412, THR 413, PRO 408, ARG 409, ASN 179, ASN 177, TYR 180, HIS 554, ARG 560, PRO 406, PHE 422	-
10	Axillarin	LEU 417	ARG 409, PRO 408, THR 416, PHE 422, ASN 557, LEU 405, ARG 560, LEU 412, THR 413	Pi-Alkyl
11	Isorhamnetin	ASP 534	PRO 408, ASN 177, TYR 180, ASN 179, ALA 553, GLY 415, THR 416, LEU 417, ASN 557, PRO 406, LEU 405	Pi-Cation, Pi-Pi T-shaped, Pi-Alkyl
12	Rhamnetin;	LEU 412, ARG 409	LEU 417, THR 416, THR 413, THR 410, ARG 560, PRO 408	Pi-Alkyl
13	Astragalin	THR 416, LEU 417, ARG 560, ASN 179	LYS 414, THR 413, LEU 412, ASN 557, PHE 422, ARG 409, PRO 408, ASP 534, ASN 177	Carbon Hydrogen bond, Pi-Pi T-shaped, Pi-Alkyl
14	Quercimeritrin	THR 416, GLY 415, ARG 560, ASN 516, PR0 514, SER 486	LEU 417, THR 413, LYS 414, LEU 412, HIS 554, THR 532, TYR 515, SER 517, ALA 487, SER 485, ASN 177, TYR 180, ASN 179, THR 410, PRO 408, ARG 409, ASN 557, ALA 553	Carbon Hydrogen bond, Pi-Pi T- T-shaped
15	Casticin	ASN 177, ASN 516, HIS 554, ARG 409	ASN 179, ARG 560, ASN 557, ALA 407, THR 410, TYR 180	Carbon Hydrogen bond, Pi-Pi Stacked, Alkyl, Pi-Alkyl
16	Artemetin	ASN 516, HIS 554, ARG 409	ASP 534, THR 532, ARG 560, ASN 557, LEU 412, LEU 417, PRO 406, PRO 408, THR 410, TYR 180, ASN 179, ASN 177	Carbon Hydrogen bond, Pi-Alkyl

17	Retusin	ASN 557	ASN 177, ASN 179, ASN 516, ASP 534, HIS 554, THR 416	Pi-Cation, Alkyl, Pi-Alkyl
18	Eupatorin	ASN 179, ASN 177, ASN 516, HIS 554, LEU 412, ARG 409	ARG 560, ASN 557, THR 416, TYR 515	Carbon-Hydrogen bond, Pi-Pi stacked, Alkyl

Table 3.9. Ligand (*Artemisia annua* GC-MS n-Hexane derived compounds) interaction with Amino acids on the target protein, 5RMM.

S/N	Ligand	HYDROGEN BONDS	VAN DER WAALS FORCES	OTHERS
1	1,8-Cyclopentadecadiyne	-	TYR 515, ASN 179, ARG 560, PRO 408, ASP 534, ASN 177, ASN 516, PRO 514	Pi-Alkyl
2	Cyclododecanone, 2-methylene-	LEU 417	HIS 554, ARG 560, ASN 557, THR 416, LEU 405, PRO 406, PHE 422, ARG 409, PRO 408	Alkyl
3	Deoxyartemisinin	HIS 554	LEU 412, PRO 406, LEU 417, ARG 560, ASN 557, THR 416	Alkyl, Pi-Alkyl

Table 3.10. Ligand (*Artemisia annua* GC-MS Dichloromethane derived compounds) interaction with Amino acids on the target protein, 5RMM

S/N	Ligand	HYDROGEN BONDS	VAN DER WAALS FORCES	OTHERS
1	2(1H)-Naphthalenone, octahydro-4a-methyl-7-(1-methylethyl)-. (4aalpha,7beta,8abeta)-	HIS 554	ARG 409, PRO 408, ARG 560, ASN 557, LEU 405	Alkyl, Pi-Alkyl
2	Civetone	HIS 554	PRO 408, ARG 560, ASN 179, ASP 534, ASN 177, ASN 516, TYR 515, PRO 514	Pi-Sigma
3	Germacrene D-4-ol	ARG 560	ASN 557, HIS 554, ASN 179, ASP 534, PRO 408, ARG 409, ALA 407, LEU 417, PRO 406, THR 416	Alkyl
4	3H-Cyclodeca[b]furan-2-one, 4,9-dihydroxy-6-methyl-3,10-dimethylene-3a,4,7,8,9,10,11,11a-3octahydro-	HIS 554, LEU 417, ASN 557	ALA 553, ARG 560, THR 416, PHE 422, GLU 418, PRO 406, ARG 409, GLY 415, THR 413	Alkyl
5	Octadecyl pentadecafluorooctanoate	HIS 554, ARG 560, LEU 417	TYR 515, ASN 177, THR 410, THR 413, ALA 553, GLY 415, LEU 405, THR 416, PHE 422, LEU 412, ARG 409, TYR 180, ASN 179	Halogen (Fluorine), Pi-Sigma, Alkyl, Pi-Alkyl

Table 3.11. Native ligand (VXG) & Nilotinib interactions with Amino acids on target protein, 5RMM.

S/N	NAME OF COMPOUNDS	HYDROGEN BONDS	VAN DER WAALS FORCES	OTHERS
1	(3S,4R)-1-acetyl-4-phenylpyrrolidine-3-carboxylic acid (VXG)	LEU 417	GLY 415, LEU 412, THR 413, THR 416, ASN 559, PHE 422, ASN 557, ARG 409, LEU 405, ASP 534	Pi-Cation, Pi-Sigma, Pi-Alkyl
2	Nilotinib	ARG 560, THR 532, ASN 177	LEU 405, PRO 514, TYR 515, ASN 179, SER 535, GLN 531, ASN 519, TYR 180, THR 410, ARG 409	Carbon-Hydrogen bond, Halogen (Fluorine), Pi-Cation, Pi-Sigma, Pi-Pi Stacked, Amide-Pi Stacked, Alkyl, Pi-Alkyl

3.4 ADME PROFILING

The ADME properties of the nineteen and eight ligands from the isolated compounds and GC-MS extracts of *Artemisia annua*, selected for ADME profiling based on binding affinity, hydrogen bond interactions with the target protein, and drug likeness potentials, are shown in Tables 12 -14.

Table 3.12. ADME properties of isolated *Artemisia annua* compounds.

S/N	Ligands	Formula	Molecu-lar weight (g/mol)	Number of hydrogen bond acceptors	Number of hydrogen bond donors	Bioavailabi-lity score	LogPo/w (MLOGP)	Drug Likeness (Lippinski)
1	Cirsiliol	$C_{17}H_{14}O_7$	330.29 g/mol	7	3	0.55	-0.07	0 violation
2	Cirsilineol	$C_{18}H_{16}O_7$	344.3 g/mol	7	2	0.55	0.17	0 violation
3	Cirsimaritin	$C_{17}H_{14}O_6$	314.29 g/mol	6	2	0.55	0.47	0 violation
4	Chlorogenic acid;	$C_{16}H_{18}O_9$	354.31 g/mol	9	6	0.11	-1.05	1 violation

5	Acacetin	$C_{16}H_{12}O_5$	284.26 g/mol	5	2	0.55	0.77	0 violation
6	Apigenin	$C_{15}H_{10}O_5$	270.24 g/mol	5	3	0.55	0.52	0 violation
7	Luteolin	$C_{15}H_{10}O_6$	286.24 g/mol	6	4	0.55	-0.03	0 violation
8	Chrysoeriol	$C_{16}H_{12}O_6$	300.26 g/mol	6	3	0.55	0.22	0 violation
9	Kaempferol	$C_{15}H_{10}O_6$	286.24 g/mol	6	4	0.55	-0.03	0 violation
10	Axillarin	$C_{17}H_{14}O_8$	346.3 g/mol	8	4	0.55	-0.59	0 violation
11	Isorhamnetin	$C_{16}H_{12}O_7$	316.26 g/mol	7	4	0.55	-0.31	0 violation
12	Rhamnetin;	$C_{16}H_{12}O_7$	316.26 g/mol	7	4	0.55	-0.31	0 violation
13	Astragalin	$C_{21}H_{20}O_{11}$	448.4 g/mol	11	7	0.17	-2.10	2 violations
14	Quercimeritrin	$C_{21}H_{20}O_{12}$	464.4 g/mol	12	8	0.17	-2.59	2 violations
15	Casticin	$C_{19}H_{18}O_8$	374.3 g/mol	8	2	0.55	-0.12	0 violation
16	Artemetin	$C_{20}H_{20}O_8$	388.4 g/mol	8	1	0.55	0.11	0 violation
17	Retusin	$C_{19}H_{18}O_7$	358.3 g/mol	7	1	0.55	0.40	0 violation
18	Eupatorin	$C_{18}H_{16}O_7$	344.3 g/mol	7	2	0.55	0.17	0 violation

Table 3.13: ADME properties of GC-MS n-Hexane-derived *Artemisia annua* compounds.

S/N	Ligand	Formula	Molecular Weight (g/mol)	Number of hydrogen bond acceptors	Number of hydrogen bond donors	Bioavailability score	Log Po/w (MLOGP) (≤ 4.15)	Drug likeness (Lippinski)
1	1,8-Cyclopentadecadiyne	$C_{15}H_{22}$	202.33 g/mol	0	0	0.55	5.54	1 violation
2	Cyclododecanone, 2-methylene-	$C_{13}H_{22}O$	194.31 g/mol	1	0	0.55	3.04	0 violation

3	Deoxyartemisinin	$C_{15}H_{22}O_4$	266.33 g/mol	4	0	0.55	2.63	0 violation

Table 3.14: ADME properties of GC-MS Dichloromethane Extract of *Artemisia annua* compounds.

S/N	Ligand	Formula	Molecular weight (g/mol)	Number of hydrogen bond acceptors	Number of hydrogen bond donors	Bioavailability score	Log Po/w (MLOGP)	Drug likeness (Lippinski)
1	2(1H)-Naphthalenone, octahydro-4a-methyl-7-(1-methylethyl)-. (4aalpha,7beta, 8abeta)-	$C_{14}H_{24}O$	208.34 g/mol	1	0	0.55	3.41	0 violation
2	Civetone	$C_{17}H_{30}O$	250.4 g/mol	1	0	0.55	4.05	0 violation
3	Germacrene D-4-ol	$C_{15}H_{26}O$	222.37 g/mol	1	1	0.55	3.56	0 violation
4	3H-Cyclodeca[b]furan-2-one, 4,9-dihydroxy-6-methyl-3,10-dimethylene-3a,4,7,8,9,10,11,11a-octahydro-	$C_{15}H_{20}O_4$	264.32 g/mol	4	2	0.55	1.53	0 violation
5	Octadecyl pentadecafluorooctanoate	$C_{26}H_{37}F_{15}O_2$	666.5 g/mol	17	0	0.17	7.86	2 violations

3.5 TOXICITY PREDICTION

The results of the ligands' different toxicity parameters (LD50, hepatotoxicity, neurotoxicity, nephrotoxicity, respiratory toxicity, cardiotoxicity, and carcinogenicity) predicted using ProTox 3.0 are shown in Tables 15-17.

Table 3.15: Toxicity profile of isolated compounds of *Artemisia annua*

S/N	Ligands	LD_{50}	Toxicity Class	Hepato-toxicity	Neuro-toxicity	Nephro-toxicity	Respiratory Toxicity	Cardio-toxicity	Carcino-genicity
1	Cirsiliol	4000mg/kg	V	-	-	+	+	-	+
2	Cirsilineol	5000mg/kg	V	-	-	+	+	-	-
3	Cirsimaritin	5000mg/kg	V	-	-	+	+	+	-
4	Chlorogenic acid;	5000mg/kg	V	-	-	+	+	-	-
5	Acacetin	4000mg/kg	V	-	-	+	+	+	-
6	Apigenin	2500mg/kg	V	-	-	+	+	-	-
7	Luteolin	3919mg/kg	V	-	-	+	+	-	+
8	Chrysoeriol	4000mg/kg	V	-	-	+	+	+	-
9	Kaempferol	3919mg/kg	V	-	-	+	+	-	-
10	Axillarin	5000mg/kg	V	-	-	+	+	+	+
11	Isorhamnetin	5000mg/kg	V	-	-	+	+	+	-
12	Rhamnetin;	5000mg/kg	V	-	-	+	+	-	+
13	Astragalin	5000mg/kg	V	-	-	+	+	-	-
14	Quercimeritrin	5000mg/kg	V	-	-	+	+	-	-
15	Casticin	5000mg/kg	V	-	-	+	+	-	-
16	Artemetin	5000mg/kg	V	-	-	+	+	-	-
17	Retusin	5000mg/kg	V	-	-	+	+	-	-
18	Eupatorin	4000mg/kg	V	-	-	+	+	-	-

Table 3.16: Toxicity profile of the GC-MS n-Hexane-derived compounds of *Artemisia annua*

S/N	Ligand	LD_{50}	Toxicity Class	Hepato-toxicity	Neuro-toxicity	Nephro-toxicity	Respiratory toxicity	Cardio-toxicity	Carcino-genicity
1	1,8-Cyclopentadecadiyne	300mg/kg	III	-	+	-	+	-	+
2	Cyclododecanone, 2-methylene-	5000mg/kg	V	-	+	-	-	-	-
3	Deoxyartemisinin	8000mg/kg	VI	-	-	-	+	+	-

Table 3.17: Toxicity profile of the GC-MS Dichloromethane derived compounds of *Artemisia annua*

S/N	Ligand	LD_{50}	Toxicity Class	Hepato-toxicity	Neuro-toxicity	Nephro-toxicity	Respiratory toxicity	Cardio-toxicity	Carcino-genicity
1	2(1H)-Naphthalenone, octahydro-4a-methyl-7-(1-methylethyl)-. (4aalpha,7beta, 8abeta)-	500 mg/kg	IV	-	+	-	-	-	-
2	Civetone	5000 mg/kg	V	-	+	-	-		-

3	Germacrene D-4-ol	3000 mg/kg	V	-	-	-	-	-
4	3H-Cyclodeca[b]furan-2-one, 4,9-dihydroxy-6-methyl-3,10-dimethylene-3a,4,7,8,9,10,11,11a-octahydro-	452 mg/kg	IV	-	-	+	+	-
5	Octadecyl pentadecafluorooctanoate	1440 mg/kg	IV	-	-	-	-	+

CHAPTER FOUR

DISCUSSION

4.1 MOLECULAR DOCKING ANALYSIS

The GC-MS analysis of hexane and dichloromethane extracts of *Artemisia annua* revealed 25 and 27 compounds, respectively, of which 3 and 5 compounds were employed for the molecular docking studies based on their high binding affinities. The isolated compounds of *Artemisia annua*, however, revealed 25 compounds, of which 18 compounds were employed for post-docking studies based on their high binding affinities with the target binding protein 5RMM.

The isolated compounds exhibited strong potential for inhibitory action against the target protein 5RMM, with docking scores ranging from -7.2 to -9.5 kcal/mol; the highest docking score was observed for Quercimeritrin. In contrast, several GC-MS-identified compounds demonstrated moderate to high binding affinities, with scores ranging from -6.6 to -7.8 kcal/mol. However, the reference standard, Nilotinib, showed a binding affinity value of -10.1kcal/mol. The ligand's stability to the protein binding site increases with an increasing negative free binding energy. As a result, the ligand-protein binding affinity improves, indicating a better activity. (Imieje and Offogah, 2025). Notably, the docking poses of Quercimeritin showed consistent interactions with key active-site residues of the 5RMM protein, including ARG560, ASN516, PRO514, and THR416. These residues, especially ARG 560, are critical to the protein's biological function. Additional van der Waals forces (LEU 417 and THR 532) and carbon–hydrogen interactions (HIS 554) further stabilize the complex, effectively "locking" the compound into the catalytic cleft and a π–π T-shaped interaction with HIS 554. The T-shaped structure is one of the lowest energy arrangements in π–π interactions; however, π- π interactions have been recognized to be pivotal to protein ligand recognition (Schaffer, 2008). It has the most conventional hydrogen bonds amongst the highlighted compounds in this group. Although their strength is weaker than that of ionic or covalent bonds, they are, in general, the predominant contributors to the specificity of molecular binding (Schaffer, 2008), indicating a favorable binding orientation and suggesting potential for functional inhibition.

Quercimeritrin, also known as Quercetin 7-O-beta-D-glucoside, is a quercetin O-glucoside where a glucosyl group is linked to position 7 of the quercetin molecule through a beta-glycosidic bond. Its potential therapeutic benefits may be linked to its aglycone, Quercetin, which is also referred to as

3,3′,4′,5,7-pentahydroxy-2-phenylchromen-4-one, a prominent example of the flavonoid subclass known as flavonols. (Di Petrillo *et al*., 2022). It has 2 benzene rings that are linked by a 3-carbon chain to form a closed pyran ring. There are a total of 5 hydroxyl groups, and glycosylation can occur on any of them, producing various quercetin glycosides by binding to glucose, xylose, or rutin.

Furthermore, the dihydroxy group between the first benzene ring, the o-dihydroxy group of the second benzene ring, and the 4-carbonyl of the closed pyran ring are the active groups present in quercetin. The biological activity of quercetin is attributed mainly to these active phenolic hydroxyl groups and double bonds. The second benzene ring in the class of natural flavonoids is the leading active site for antioxidant and reactive oxygen species (ROS) scavenging, which can potentiate the activity of Quercetin in this case against SARS-CoV-2 (Wang *et al*., 2022). Quercetin also demonstrated noteworthy inhibitory activity against other major therapeutic targets of SARS-CoV-2, such as the 3-chymotrypsin-like protease(3CLpro), papain-like protease (PLpro), RNA-dependent RNA polymerase, and the spike (S) protein. It has been reported to have a theoretical, but significant, capacity to interfere with SARS-CoV-2 replication, with a study showing it ranked fifth among 18 candidates tested. (Derosa *et al.,* 2019). These studies lay the proper foundation for explaining its significantly high binding affinity for 5RMM.

Similarly, the compound with the second-highest binding affinity, Rhamnetin, exhibited notable interactions with residues such as LEU412, ARG409, LEU417, THR416, THR413, THR410, ARG560, and PRO408. These interactions were stabilized by carbon-hydrogen bonds and π-alkyl interactions, as illustrated in the 2D and 3D molecular visualizations shown in Figures 8 and 9. Rhamnetin, an O-methylated variant of the flavonol quercetin, is classified within the flavonol subclass and has the chemical formula $C_{16}H_{12}O_7$. Its molecular configuration can be characterized as 2-(3,4-dihydroxyphenyl)-3,5-dihydroxy-7-methoxychromen-4-one. Important structural characteristics include the presence of hydroxyl groups at the 3, 3′, and 4′ positions on the phenyl ring and chromone core, a methoxyl group situated at position 7 on the A ring, and a hydrogen atom located at position 5. These structural features are integral to rhamnetin's distinct pharmacological characteristics. The hydroxyl groups are crucial in the process of scavenging free radicals, offering strong antioxidant properties by neutralizing harmful reactive species.

Meanwhile, the methoxyl group at position 7 enhances the molecule's lipophilicity, increasing its ability to permeate cell membranes and improving its metabolic stability compared to non-

methoxylated flavonoids like quercetin (Adbel-Rasol *et al.*, 2025). However, their planar, polyphenolic scaffolds with multiple hydroxyl groups ensure optimal surface complementarity and a balanced hydrophilic/hydrophobic profile. The flat aromatic rings slide snugly between hydrophobic regions, and the –OH groups form directional polar contacts, minimizing entropic penalties upon binding. Together, this combination of diverse interaction types, targeted residue engagement, and molecular rigidity drives down the overall binding free energy, accounting for their superior docking scores.

In comparison, Deoxyartemisinin and 3H-Cyclodeca[b]furan-2-one, 4,9-dihydroxy-6-methyl-3,10-dimethylene-3a,4,7,8,9,10,11,11a-octahydro-, the compounds with the highest binding affinities from the GC-MS n-hexane and dichloromethane extracts, respectively, also demonstrated favorable interactions with the 5RMM protein, engaging several overlapping residues. Deoxyartemisinin interacted with HIS554, LEU412, PRO406, LEU417, ARG560, ASN557, and THR416, while 3H-Cyclodeca[b]furan-2-one, 4,9-dihydroxy-6-methyl-3,10-dimethylene-3a,4,7,8,9,10,11,11a-octahydro- formed contacts with HIS554, LEU417, ASN557, ALA553, ARG560, THR416, PHE422, and GLU418, as illustrated in the in 2D and 3D molecular visualizations presented in Figures 10 and 11.

However, the interaction profiles differed like their non-covalent forces. Deoxyartemisinin primarily relied on hydrogen bonds, van der Waals forces, and alkyl/π-alkyl interactions, consistent with its hydrophobic character. Notably, it formed a π-alkyl interaction with HIS 554 and an alkyl contact with ALA 553, contributing to efficient shape complementarity and a low entropic penalty. These features likely account for its slightly more favorable docking score (−7.8 kcal/mol). In contrast, 3H-Cyclodeca[b]furan-2-one, 4,9-dihydroxy-6-methyl-3,10-dimethylene-3a,4,7,8,9,10,11,11a-octahydro- engaged in a less diverse interaction network, stabilizing its interaction with the active site of the receptor mainly by hydrogen bonds with HIS 554, ASN 557, and LEU 417, and an alkyl contact with LEU 412. However, its greater conformational flexibility may have been reflected in a slightly lower docking score (−7.7 kcal/mol). Deoxyartemisinin is a metabolite of the artemisinin biotransformation process and has a relatively low yield during extraction. Also, the lack of the endoperoxide functional group, which is essential for antimalarial activity, has not garnered attention in research related to potential biological functions, as evidenced by the limited number of reports over the years. Artemisinin exerts its biological activity through an endoperoxide bridge present in

its structure, although deoxyartemisinin loses this endoperoxide group after metabolization. Studies such as (Favero *et al*., 2024) have demonstrated that it still has biological activity despite the loss of the active functional group. In other words, Deoxyartemisinin chemically resembles artemisinin, the lactone without the endoperoxide moiety. This may also be one of the reasons for its favourable docking scores.

Importantly, residues such as HIS 554, LEU 417, ARG 560, and ASN 557 were commonly targeted across all four compounds, indicating a conserved and functionally relevant binding pocket that may serve as a strategic anchor for future ligand optimization.

Despite their differences, the consistent targeting of key residues reinforces the therapeutic relevance of the binding site and supports the potential of these natural and semi-synthetic compounds as promising antiviral candidates against the 5RMM protein. The comparative analysis suggests that while isolated compounds tend to exhibit more defined and potent interactions, certain GC-MS constituents may contribute to a broader spectrum of binding profiles, potentially offering synergistic effects when combined. These findings provide a foundational basis for further exploration of *Artemisia annua*'s phytochemical inventory as a source of antiviral agents targeting the 5RMM protein.

Nilotinib, a tyrosine kinase inhibitor with reported antiviral activity, was employed as a reference compound in this study due to its previously demonstrated efficacy against SARS-CoV-2 targets, established safety profile for human use at therapeutic doses, and its relatively well-tolerated profile.The established safety profile for human use at therapeutic doses indicates that it is relatively well-tolerated. Additionally, in silico repurposing research revealed that nilotinib attaches to the receptor-binding domain of the SARS-CoV-2 spike protein, potentially blocking entry into host cells through the ACE2 receptor. Additional *in silico* studies are still ongoing to understand the interactions between tyrosine kinase inhibitors and SARS-CoV-2 and elucidate the mechanism of action. (Cagno *et al*., 2020).

Nilotinib exhibited a docking score of −10.1 kcal/mol against the 5RMM protein, serving as a benchmark for evaluating the binding affinities of the test compounds. Nilotinib interacted with the target protein amino acid residues ARG 560, ASN 177, and ASN 179 via conventional hydrogen bonds, ASP 534 via a Carbon-hydrogen bond, and a π-π stacked bond with HIS 554. Considering

that, ARG 560, ASN 177, and ASP 534 are key amino acid residues at the binding site of the 5RMM protein; these interactions may be responsible for its high binding affinity. The isolated compounds previously addressed exhibited docking scores approaching those of Nilotinib, while the GC-MS-derived compounds exhibited lower binding scores than the standard. However, the compounds and the standard all interact with key amino acid residues such as ARG 560 and HIS 554, suggesting strong interaction potential with the target protein and reinforcing their candidacy for further antiviral development.

4.2 ADME PROFILING

Pharmacokinetic events, including absorption, distribution, metabolism, and excretion (ADME), the route of drug targets, and drug interactions in the body. Consequently, when designing novel therapeutic agents, pharmacokinetic parameters must be considered (Imieje and Offogah, 2025). To evaluate the drug-likeness and pharmacokinetic suitability of Artemisia annua compounds against the 5RMM protein, four primary descriptors were analyzed: hydrogen bond donors (HBD), hydrogen bond acceptors (HBA), bioavailability score, and MLOGP values. These parameters offer insight into oral bioavailability, membrane permeability, and overall therapeutic potential.

Although various criteria exist for predicting drug-likeness, this study employed **Lipinski's Rule of Five**, a widely accepted guideline for evaluating the oral bioavailability of small-molecule drugs. According to this rule, an orally active compound should not violate more than one of the following four parameters: (Lippinski *et al*., 2001)

- **Molecular weight (MW):**

It should be less than **500 Daltons** to ensure efficient membrane permeability.

- **Hydrogen bond donors (HBD):**

Should be **≤ 5** (typically –OH and –NH groups), as excessive donors are commonly believed to reduce lipophilicity and hinder absorption.

- **Hydrogen bond acceptors (HBA):**

Should be **≤ 10** (typically oxygen and nitrogen atoms), since high polarity can impair passive diffusion.

- **Octanol-water partition coefficient (Log P):** Should be **≤ 5**, indicating balanced lipophilicity for membrane transport without compromising solubility. MLOGP is one of the models SwissADME uses to estimate a compound's lipophilicity. It is a topological method based on a linear relationship with 13 implemented molecular descriptors (Nagsen *et al*., 2023). Ideal drug candidates typically fall within the range of **MLOGP ≤ 4.15**, as per SwissADME's drug-likeness criteria. Compounds with excessively high MLOGP values may suffer from poor solubility or toxicity, while those with very low values may struggle with membrane permeability.

Included in the ADME analysis for this study is the oral bioavailability score, although not one of the original four. SwissADME's bioavailability score integrates Lipinski's criteria with Veber's rules (rotatable bonds, polar surface area) to predict whether oral bioavailability exceeds ~10% (Ranjith and Ranvikumar, 2019). A score **≥ 0.55** flags molecules likely to meet RO5 thresholds and achieve an acceptable %F.

In this study, out of the 18 Isolated compounds analyzed, 16 satisfied the Lipinski criteria, indicating favorable drug-like characteristics, while 3 compounds violated more than one parameter and were considered non-compliant. Of the two highest-scoring compounds that were previously discussed, Rhamnetin passed the Lippinski drug likeness filter, while Quercimeritrin had 2 violations. This might be as a result of Rhamnetin's peculiar structure, especially the methoxylation at position 7 of its first benzene ring, which has been stated prior as responsible for enhancing the molecule's lipophilicity, increasing its ability to permeate cell membranes and improving its metabolic stability compared to non-methoxylated flavonoids like quercetin and its glycosides in this case, such as Quercimeritrin and making it particularly important in Rhamnetin's pharmacokinetics and pharmacodynamics. The violations shown by Quercimeritrin do not make it any less of a potential lead compound for further study. This filter mainly shows that it may not be therapeutically viable as an oral drug; however, other routes of administration for its activity can also be explored.

For the GC-MS Hexane extract, 2 out of the 3 identified compounds passed the drug-likeness filter, whereas 1 compound failed due to violations. Deoxyartemisinin was one of the compounds that passed this filter, thereby highlighting it as a potential orally available lead compound.

In contrast, all 3 compounds identified from the GC-MS Dichloromethane extract met the Lipinski criteria, including 3H-Cyclodeca[b]furan-2-one,4,9-dihydroxy-6-methyl-3,10-dimethylene-

3a,4,7,8,9,10,11,11a-octahydro-, suggesting strong potential for oral bioavailability and further pharmacological development.

4.3 TOXICITY PREDICTION

Toxicity profiling is a critical component of early-stage drug development, as it helps identify potential safety risks before clinical evaluation. While a compound may exhibit strong binding affinity and favorable pharmacokinetic properties, its therapeutic viability ultimately depends on its safety profile. The toxicity profile parameters focused on in this study included LD50 (mg/kg), predicted toxicity class, hepatoxicity, respiratory toxicity, carcinogenicity, nephrotoxicity, and neurotoxicity. Toxicity levels are classified as follows: classes 1 and 2 (fatal if swallowed, LD50 ≤ 5 & LD50 ≤ 50, respectively), class 3 (toxic if swallowed, LD50 ≤ 300), class 4 (harmful if swallowed, LD50 ≤ 2000), class 5 (may be harmful if swallowed, LD50 ≤ 5000), and class 6 (non-toxic, (LD50 > 5000) (Imieje and Offogah,2025). As shown in Table 15, all isolated compounds were predicted to fall into toxicity class 5, indicating they may be harmful if swallowed. As stated earlier regarding Quercimeritrin, this may require consideration of alternative routes of administration for therapeutic use during drug development and lead optimization.

In contrast, the GC-MS extracts (Tables 16 and 17) exhibited a broader toxicity profile. Specifically, three compounds were classified as harmful if swallowed (class 4), three compounds as may be harmful if swallowed (class 5), one compound as non-toxic (class 6), and one compound as toxic if swallowed (class 3). The compound Deoxyartemisinin was classified as non-toxic, further highlighting its safety profile and establishing it as a significant potential lead compound that could yield breakthrough insights if further studied.

This variation suggests that while isolated compounds show consistent toxicity levels, the GC-MS-derived phytochemicals display a wider range of safety profiles, which may influence their therapeutic applicability and dosage considerations.

CHAPTER FIVE

CONCLUSION

This study aimed to evaluate the antiviral potential of the phytochemical constituents of *Artemisia annua* against the viral helicase 5RMM, a highly conserved protein primarily responsible for viral replication, comparing the activity of its isolated compounds and GC-MS-derived compounds using molecular docking and computational analysis. At the end of the study, various compounds from each group exhibited promising binding affinities and secure interactions with the active site of 5RMM, suggesting potential inhibitory effects.

Notably, the isolated compounds Quercimeritrin and Rhamnetin exhibited ideal binding affinity scores, which were comparable to that of the standard, Nilotinib. Moreover, their performance surpassed that of the highest-scoring compounds from the GC-MS n-hexane and dichloromethane extracts of *Artemisia annua*. This was expected to some extent; however, the binding affinity scores of the GC-MS compounds suggest promising antiviral activity against 5RMM.

While this study suggests that the phytochemicals in *Artemisia annua* exhibit antiviral potential against the viral protein 5RMM, it is imperative to note that *in-silico* studies are mainly investigational and only suggest the therapeutic potential of these highlighted compounds. Therefore, this study could serve as a foundational study for further investigation, possibly via in vitro assays, into the antiviral activity of *Artemisia annua* against the viral protein of interest.

In the end, these results once again affirm the therapeutic potential of *Artemisia annua* as a lead source of bioactive phytochemicals with latent antiviral activity, thus further highlighting its relevance in modern drug discovery.

REFERENCES

Abdel-Rasol, M. A., Al-Hamadani, M. Y. I., Ibrahim, Z. A., & El-Sayed, W. M. (2025). Rhamnetin is a multifaceted flavonoid with potential in cancer therapy: Current insights and future directions. *Future Journal of Pharmaceutical Sciences*, 11, 140. https://doi.org/10.1186/s43094-025-00887-3

Aleem, A., & Kothadia, J. P. (2025). Remdesivir. In *StatPearls* [Internet]. StatPearls Publishing. https://www.ncbi.nlm.nih.gov/books/NBK563261/

Anibogwu, R., Jesus, K., Pradhan, S., Pashikanti, S., Mateen, S., & Sharma, K. (2021). Extraction, Isolation and Characterization of Bioactive Compounds from *Artemisia* and Their Biological Significance: A Review. *Molecules (Basel, Switzerland)*, *26*(22), 6995. https://doi.org/10.3390/molecules26226995

Artemisia annua. (2025, August 16). In *Wikipedia: The Free Encyclopedia*. Retrieved August 27, 2025, from https://en.wikipedia.org/wiki/Artemisia_annua

Atanasov, A. G., Waltenberger, B., Pferschy-Wenzig, E. M., Linder, T., Wawrosch, C., Uhrin, P., Temml, V., Wang, L., Schwaiger, S., Heiss, E. H., Rollinger, J. M., Schuster, D., Breuss, J. M., Bochkov, V., Mihovilovic, M. D., Kopp, B., Bauer, R., Dirsch, V. M., & Stuppner, H. (2015). Discovery and resupply of pharmacologically active plant-derived natural products: A review. *Biotechnology Advances, 33*(8), 1582–1614. https://doi.org/10.1016/j.biotechadv.2015.08.001

Baggieri, M., Gioacchini, S., Borgonovo, G., Catinella, G., Marchi, A., Picone, P., et al. (2023). Antiviral, virucidal and antioxidant properties of Artemisia annua against SARS-CoV-2. *Biomedicine & Pharmacotherapy*, 168, 115682. https://doi.org/10.1016/j.biopha.2023.115682

Banerjee, P., Kemmler, E., Dunkel, M., & Preissner, R. (2024). ProTox 3.0: A webserver for the prediction of toxicity of chemicals. *Nucleic Acids Research*, 52(W1), W513–W520. https://doi.org/10.1093/nar/gkae303

Barcelos, M. P., Gomes, S. Q., Federico, L. B., Francischini, I. A. G., Hage-Melim, L. I. da S., Silva, G. M., & de Paula da Silva, C. H. T. (2022). Lead optimization in drug discovery. In *Research Topics in Bioactivity, Environment and Energy* (pp. 481–500). Springer. https://doi.org/10.1007/978-3-031-15707-3_20

Batool, M., Ahmad, B., & Choi, S. (2019). A Structure-Based Drug Discovery Paradigm. *International journal of molecular sciences*, *20*(11), 2783. https://doi.org/10.3390/ijms20112783

Berman, H. M., Westbrook, J., Feng, Z., Gilliland, G., Bhat, T. N., Weissig, H., Shindyalov, I. N., & Bourne, P. E. (2000). The Protein Data Bank. *Nucleic Acids Research*, 28(1), 235–242. https://doi.org/10.1093/nar/28.1.235

Borole, P. G., & Khadse, A. N. (2024). ADMET Predictor – An overview of prediction and evaluation of ADMET properties of drugs and chemicals. *International Journal of Scientific Development and Research*, 9(3), 128–133. https://www.ijsdr.org/papers/IJSDR2403028.pdf

Cagno, V., Magliocco, G., Tapparel, C., & Daali, Y. (2020). The tyrosine kinase inhibitor nilotinib inhibits SARS-CoV-2 in vitro. *Basic & Clinical Pharmacology & Toxicology*, 128(4), 702–707. https://doi.org/10.1111/bcpt.13537

Cao, R., Hu, H., Li, Y., Wang, X., Xu, M., Liu, J., et al. (2020). Anti-SARS-CoV-2 potential of artemisinins in vitro. *ACS Infectious Diseases*, 6(9), 2524–2531. https://doi.org/10.1021/acsinfecdis.0c00522

Chen, J., Malone, B., Llewellyn, E., Grasso, M., Shelton, P. M. M., Olinares, P. D. B., Maruthi, K., Eng, E. T., Vatandaslar, H., Chait, B. T., Kapoor, T. M., Darst, S. A., & Campbell, E. A. (2020). Structural basis for helicase-polymerase coupling in the SARS-CoV-2 replication-transcription complex. *Cell, 182*(6), 1560–1573.e13. https://doi.org/10.1016/j.cell.2020.07.033

Corona, A., Wycisk, K., Talarico, C., Manelfi, C., Milia, J., Cannalire, R., Esposito, F., Gribbon, P., Zaliani, A., Iaconis, D., Beccari, A. R., Summa, V., Nowotny, M., & Tramontano, E. (2022). Natural compounds inhibit SARS-CoV-2 nsp13 unwinding and ATPase enzyme activities. ACS *Pharmacology & Translational Science*, 5(4), 226–239. https://doi.org/10.1021/acsptsci.2c00025

Daina, A., Michielin, O., & Zoete, V. (2017). SwissADME: A free web tool to evaluate pharmacokinetics, drug-likeness and medicinal chemistry friendliness of small molecules. *Scientific Reports*, 7, 42717. https://doi.org/10.1038/srep42717

Dassault Systèmes. (2025). *BIOVIA Discovery Studio FAQ* [Internet]. San Diego, CA: Dassault Systèmes. Retrieved September 5, 2025, from https://www.3ds.com/products-services/biovia/resources/biovia-discovery-studio-faq

Derosa, G., Maffioli, P., D'Angelo, A., & Di Pierro, F. (2021). A role for quercetin in coronavirus disease 2019 (COVID-19). *Phytotherapy Research*, 35(3), 1230–1236. https://doi.org/10.1002/ptr.6887

Di Petrillo, A., Germano, O., Antonella, F., Massimo, C. F., (2022). Quercetin and its derivatives as antiviral potentials: A comprehensive review. *Phytotherapy Research*, 36(1), 266–278. https://doi.org/10.1002/ptr.7309

Eberhardt, J., Santos-Martins, D., Tillack, A. F., & Forli, S. (2021). AutoDock Vina 1.2.0: New docking methods, expanded force field, and Python bindings. *Journal of Chemical Information and Modeling*, 61(8), 3891–3898. https://doi.org/10.1021/acs.jcim.1c00203

El-Daly, M. M. (2024). Advances and challenges in SARS-CoV-2 detection: A review of molecular and serological technologies. *Diagnostics*, 14(5), 519. https://doi.org/10.3390/diagnostics14050519

Emrani, J., Ahmed, M., Jeffers-Francis, L., Teleha, J. C., Mowa, N., Newman, R. H., & Thomas, M. D. (2021). SARS-COV-2 infection, transmission, transcription, translation, proteins, and treatment: A review. *International Journal of Biological Macromolecules, 193*(Pt B), 1249–1273. https://doi.org/10.1016/j.ijbiomac.2021.10.172

European Centre for Disease Prevention and Control. (2025, August 24). *SARS-CoV-2 variants of concern and variants under monitoring*. https://www.ecdc.europa.eu/en/covid-19/variants-concern

Favero, F. de F., Basting, R. T., de Freitas, A. S., Rabelo, L. da S. D., Nonato, F. R., Zafred, R. R. T., de Oliveira Sousa, I. M., Queiroz, N. de C. A., Napimoga, J. T. C., de Carvalho, J. E., & Foglio, M. A. (2024). Artemisinin and deoxyartemisinin isolated from *Artemisia annua* L. promote distinct antinociceptive and anti-inflammatory effects in an animal model. *Biomedicine & Pharmacotherapy*, 178, 117299. https://doi.org/10.1016/j.biopha.2024.117299

Ferreira, L. G., Dos Santos, R. N., Oliva, G., & Andricopulo, A. D. (2015). Molecular docking and structure-based drug design strategies. *Molecules*, 20(7), 13384–13421. https://doi.org/10.3390/molecules200713384

Forli, S., Huey, R., Pique, M. E., Sanner, M. F., Goodsell, D. S., & Olson, A. J. (2016). Computational protein-ligand docking and virtual drug screening with the AutoDock suite. *Nature Protocols*, 11(5), 905–919. https://doi.org/10.1038/nprot.2016.051

Fuzimoto, A. D. (2021). An overview of the anti-SARS-CoV-2 properties of Artemisia annua, its antiviral action, protein-associated mechanisms, and repurposing for COVID-19 treatment. *Journal of Integrative Medicine*, 19(5), 375–388. https://doi.org/10.1016/j.joim.2021.07.003

Ghersi, D., & Sanchez, R. (2009). Improving accuracy and efficiency of blind protein-ligand docking by focusing on predicted binding sites. *Proteins*, 74(2), 417–424. https://doi.org/10.1002/prot.22154

Ghose, A. K., Viswanadhan, V. N., & Wendoloski, J. J. (1999). A knowledge-based approach in designing combinatorial or medicinal chemistry libraries for drug discovery. 1. A qualitative and quantitative characterization of known drug databases. *Journal of Combinatorial Chemistry*, 1(1), 55–68.

Gu, J., & Korteweg, C. (2007). Pathology and pathogenesis of severe acute respiratory syndrome. *The American Journal of Pathology, 170*(4), 1136–1147. https://doi.org/10.2353/ajpath.2007.061088

Hameduh, T., Haddad, Y., Adam, V., & Heger, Z. (2020). Homology modeling in the time of collective and artificial intelligence. *Computational and Structural Biotechnology Journal*, 18, 3494–3506. https://doi.org/10.1016/j.csbj.2020.11.007

Hu, B., Guo, H., Zhou, P., Zheng-Li, S. (2021). Characteristics of SARS-CoV-2 and COVID-19. *Nature Reviews Microbiology*, 19, 141–154. https://doi.org/10.1038/s41579-020-00459-7

Imieje, V. O., & Offogah, C. O. (2025). In silico evaluation of potential antimalarial phytoconstituents from two medicinal plants used in Nigerian ethnomedicine. *Journal of Pharmacy and Allied Sciences*, 22(1), 4567–4574.

Juurlink, D. N. (2020). Safety considerations with chloroquine, hydroxychloroquine, and azithromycin in the management of SARS-CoV-2 infection. *CMAJ, 192*(15), E450–E453. https://doi.org/10.1503/cmaj.200528

Kannan, C., Radhakrishnan, S., Sambathkumar, R., Dhanaraja, D., Muvendhiran, S., & Dharnisha, N. J. (2025). A review on step into the future: Python Prescription (PyRx) transforms virtual drug discovery with AI-driven tools. *African Journal of Biomedical Research*, 27(3S). https://doi.org/10.53555/AJBR.v27i3S.2119

Khailany, R. A., Safdar, M., & Ozaslan, M. (2020). Genomic characterization of a novel SARS-CoV-2. *Gene Reports*, 19, 100682. https://doi.org/10.1016/j.genrep.2020.100682

Kim, S. (2019). Public chemical databases. In S. Ranganathan, M. Gribskov, K. Nakai, & C. Schönbach (Eds.), *Encyclopedia of Bioinformatics and Computational Biology* (1st ed., pp. 628–639). Academic Press. https://doi.org/10.1016/B978-0-12-809633-8.20192-1

Kinghorn, A. D., Pan, L., Fletcher, J. N., & Chai, H. (2011). The relevance of higher plants in lead compound discovery programs. *Journal of Natural Products*, 74(6), 1539–1555. https://doi.org/10.1021/np200391c

Kloskowski, P., Neumann, P., Kumar, P., Berndt, A., Dobbelstein, M., & Ficner, R. (2025). Myricetin-bound crystal structure of the SARS-CoV-2 helicase NSP13 facilitates the discovery of novel natural inhibitors. *Acta Crystallographica Section D: Structural Biology*, 81, 310–326. https://doi.org/10.1107/S2059798325004498

Lim, A. W. Y., Schneider, L., & Loy, C. (2024). Galantamine for dementia due to Alzheimer's disease and mild cognitive impairment. *Cochrane Database of Systematic Reviews*, 11(11), CD001747. https://doi.org/10.1002/14651858.CD001747.pub4

Lionta, E., Spyrou, G., Vassilatis, D. K., & Cournia, Z. (2014). Structure-based virtual screening for drug discovery: principles, applications and recent advances. *Current topics in medicinal chemistry*, *14*(16), 1923–1938. https://doi.org/10.2174/1568026614666140929124445

Lipinski, C. A., Lombardo, F., Dominy, B. W., & Feeney, P. J. (2001). Experimental and computational approaches to estimate solubility and permeability in drug discovery and

development settings. *Advanced Drug Delivery Reviews*, 46(1–3), 3–26. https://doi.org/10.1016/S0169-409X(00)00129-0

Meng, X. Y., Zhang, H. X., Mezei, M., & Cui, M. (2011). Molecular docking: A powerful approach for structure-based drug discovery. *Current Computer-Aided Drug Design*, 7(2), 146–157. https://doi.org/10.2174/157340911795677602

Muralidar, S., Ambi, S. V., Sekaran, S., & Krishnan, U. M. (2020). The emergence of COVID-19 as a global pandemic: Understanding the epidemiology, immune response and potential therapeutic targets of SARS-CoV-2. *Biochimie, 179*, 85–100. https://doi.org/10.1016/j.biochi.2020.09.018

Nagsen, A., Kamble, S., & Mitkar, A. A. (2023). Swiss ADME predictions of pharmacokinetics and drug-likeness properties of secondary metabolites present in *Trigonella foenum-graecum*. *Journal of Pharmacognosy and Phytochemistry*, 12(5), 341–349. https://doi.org/10.22271/phyto.2023.v12.i5d.14745

Nasim, N., Sandeep, I. S., & Mohanty, S. (2022). Plant-derived natural products for drug discovery: Current approaches and prospects. *The Nucleus*, 65(3), 399–411. https://doi.org/10.1007/s13237-022-00405-3

Newman, D. J., & Cragg, G. M. (2012). Natural products as sources of new drugs over the 30 years from 1981 to 2010. *Journal of Natural Products*, 75(3), 311–335. https://doi.org/10.1021/np200906s

Newman, J. A., Douangamath, A., Yadzani, S., Yosaatmadja, Y., Aimon, A., Brandão-Neto, J., Dunnett, L., Gorrie-Stone, T., Skyner, R., Fearon, D., Schapira, M., von Delft, F., & Gileadi, O. (2021). Structure, mechanism and crystallographic fragment screening of the SARS-CoV-2 NSP13 helicase. *Nature Communications, 12*(1), 4848. https://doi.org/10.1038/s41467-021-25166-6

Niazi, S. K., & Mariam, Z. (2023). Computer-aided drug design and drug discovery: A prospective analysis. *Pharmaceuticals*, 17(1), 22. https://doi.org/10.3390/ph17010022

Patel, T. K., Patel, P. B., Barvaliya, M., Saurabh, M. K., Bhalla, H. L., & Khosla, P. P. (2021). Efficacy and safety of lopinavir-ritonavir in COVID-19: A systematic review of randomized

controlled trials. *Journal of Infection and Public Health*, 14(6), 740–748. https://doi.org/10.1016/j.jiph.2021.03.015

Pillai, O., Dhanikula, A. B., & Panchagnula, R. (2001). Drug delivery: An odyssey of 100 years. *Advanced Drug Delivery Reviews*, 46(1–3), 3–20. https://doi.org/10.1016/S1367-5931(00)00226-X

Purohit, D., Makhija, M., Pandey, P., Kumar, S., Dutt, R., Kaushik, D., Kumar, P., & Kumar, S. (2022). Role of computer-aided drug design in the discovery and development of new medicinal agents: A review. *Journal of Medical and Pharmaceutical Allied Sciences*, 11(3), 2300. https://doi.org/10.55522/jmpas.V11I3.230

Ranjith, D., & Ravikumar, C. (2019). SwissADME predictions of pharmacokinetics and drug-likeness properties of small molecules present in *Ipomoea mauritiana Jacq. Journal of Pharmacognosy and Phytochemistry*, 8(5), 2063–2073.

Schaeffer, L. (2008). The role of functional groups in drug receptor interactions. In R. Mannhold, H. Kubinyi, & G. Folkers (Eds.), *The Practice of Medicinal Chemistry* (3rd ed., pp. 359–377). Elsevier.

Schake, P., Bolz, S. N., Linnemann, K., & Schroeder, M. (2025). PLIP 2025: Introducing protein–protein interactions to the protein–ligand interaction profiler. *Nucleic Acids Research*, 53(W1), W463–W465. https://doi.org/10.1093/nar/gkaf361

Septembre-Malaterre, A., Lalarizo Rakoto, M., Marodon, C., Bedoui, Y., Nakab, J., Simon, E., Hoarau, L., Savriama, S., Strasberg, D., Guiraud, P., Selambarom, J., & Gasque, P. (2020). Artemisia annua, a traditional plant brought to light. *International Journal of Molecular Sciences*, 21(14), 4986. https://doi.org/10.3390/ijms21144986

Sharma, V., Wakode, S., & Kumar, H. (2021). Structure- and ligand-based drug design: Concepts, approaches, and challenges. In *Chemoinformatics and Bioinformatics in the Pharmaceutical Sciences* (pp. 27–53). Elsevier. https://doi.org/10.1016/B978-0-12-821748-1.00004-X

Stanzione, F., Giangreco, I., & Cole, J. C. (2021). Use of molecular docking computational tools in drug discovery. In D. R. Witty & B. Cox (Eds.), *Progress in Medicinal Chemistry* (Vol. 60, pp. 273–343). Elsevier. https://doi.org/10.1016/bs.pmch.2021.01.004

Swamikannu, B., Umapathy, V. R., Natarajan, P. M., Nandini, M. S., Queency Stylin, A. G. S., Vimalarani, V., & Rajinikanth, S. (2024). Unlocking the therapeutic benefits of *Artemisia annua*: A comprehensive overview of its medicinal properties. *Journal of Pharmacy and Bioallied Sciences,* 16(Suppl 5), S4248–S4253. https://doi.org/10.4103/jpbs.jpbs_1250_24

Turner, A. J. (2015). ACE2 cell biology, regulation, and physiological functions. In *The Protective Arm of the Renin Angiotensin System (RAS)* (pp. 185–189). https://doi.org/10.1016/B978-0-12-801364-9.00025-0

Ursu, O., Rayan, A., Goldblum, A., & Oprea, T. (2011). Understanding drug-likeness. *Wiley Interdisciplinary Reviews: Computational Molecular Science*, 1(5), 760–781. https://doi.org/10.1002/wcms.52

Veber, D. F., Johnson, S. R., Cheng, H. Y., Smith, B. R., Ward, K. W., & Kopple, K. D. (2002). Molecular properties that influence the oral bioavailability of drug candidates. *Journal of Medicinal Chemistry*, 45(12), 2615–2623.

Verma, M. K., Sharma, S., & Kumar, S. (2020). A review on pharmacological properties of Artemisia annua. *Journal of Pharmacognosy and Phytochemistry*, 9(6), 2179–2183. https://www.phytojournal.com/archives/2020/vol9issue6/PartAE/10-2-151-657.pdf

Wang, G., Wang, Y., Yao, L., Gu, W., Zhao, S., Shen, Z., Lin, Z., Liu, W., & Yan, T. (2022). Pharmacological activity of quercetin: An updated review. *Evidence-Based Complementary and Alternative Medicine*, Article ID 3997190. https://doi.org/10.1155/2022/3997190

Wang, M., Cao, R., Zhang, L., et al. (2020). Remdesivir and chloroquine effectively inhibit the recently emerged novel coronavirus (2019-nCoV) in vitro. *Cell Research, 30*, 269–271. https://doi.org/10.1038/s41422-020-0282-0

World Health Organization. (2025, August 24). *Coronavirus disease (COVID-19) Fact sheets*. https://www.who.int/news-room/fact-sheets/detail/coronavirus-disease-(covid-19)

Xie, X., Zhong, Z., Zhao, W., Zheng, C., Wang, F., & Liu, J. (2020). Chest CT for Typical Coronavirus Disease 2019 (COVID-19) Pneumonia: Relationship to Negative RT-PCR Testing. *Radiology*, *296*(2), E41–E45. https://doi.org/10.1148/radiol.2020200343

Yan, L., Zhang, Y., Ge, J., Zheng, L., Gao, Y., Wang, T., Jia, Z., Wang, H., Huang, Y., Li, M., Wang, Q., Rao, Z., & Lou, Z. (2020). Architecture of a SARS-CoV-2 mini replication and transcription complex. *Nature communications*, *11*(1), 5874. https://doi.org/10.1038/s41467-020-19770-1